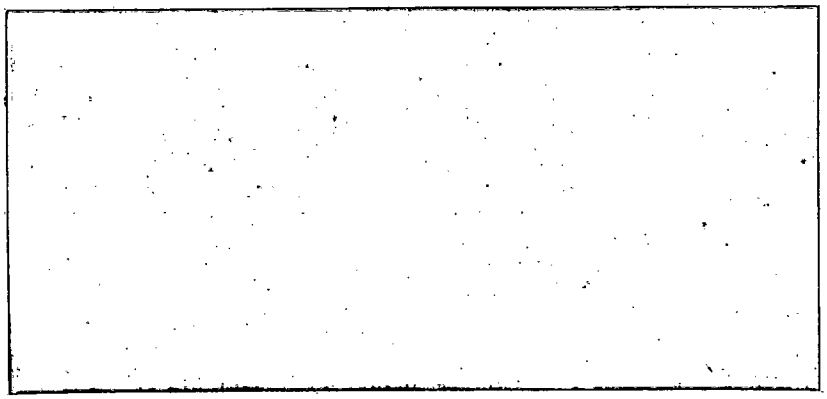

Materials Science Center

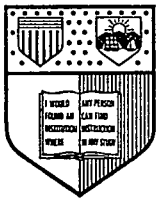

Cornell University

ITHACA, NEW YORK

DISCLAIMER

This report has been prepared by the Central Report Facility of the Materials Science Center.

COO-3150-2
Report #1770

ELECTRICAL AND THERMAL TRANSPORT PROPERTIES OF TUNGSTEN AND THE RF SIZE EFFECT IN POTASSIUM

by

David Kendall Wagner

Ph. D. Thesis
November 1971

Research Group:
Prof. R. Bowers
LASSP

THIS PAGE
WAS INTENTIONALLY
LEFT BLANK

ACKNOWLEDGMENTS

Many members of the Cornell Physics department have been helpful to me, both directly and indirectly. J. W. Wilkins and B. W. Maxfield have been especially generous in making available their time for discussions of aspects of this work, and their interest in this work has been greatly appreciated. J. C. Garland was responsible for the initial stages of the zero-field tungsten work. Much of this preliminary work was useful in developing the final design of the experiment. D. Baer patiently assisted with a number of the tungsten experiments and B. Addis zone-refined the tungsten samples used in this study. H. Taub and G. A. Stringer did much of the preliminary work on the rf size effect. The care and thought that they devoted to designing the experiment and developing the necessary experimental techniques were an invaluable aid in the continuation of this project. My special committee chairman, R. Bowers, has provided encouragement and guidance, and has contributed enormously in making my years as a graduate student both rewarding and enjoyable. It has been a privilege to be one of his students.

I am also greatly indebted to Conyers Herring, who provided much of the motivation for the experimental as well as the theoretical work presented in this thesis. In addition, his correpondence on certain aspects of the theory proved to be very valuable.

The work reported here has been supported by the Atomic Energy Commission under contract AT(11-1)-3150, COO-3150-2 and by the Advanced Research Projects Agency through the use of the facilities of the Materials Science Center, Cornell University.

TABLE OF CONTENTS

Chapter		Page
I	INTRODUCTORY REMARKS.	1
II	LOW-TEMPERATURE ELECTRICAL AND THERMAL RESISTIVITIES OF TUNGSTEN	4
	A. Introduction.	4
	B. Experimental Details.	8
	C. Experimental Results.	13
	D. Discussion.	20
III	LATTICE THERMAL CONDUCTIVITY AND HIGH-FIELD ELECTRICAL AND THERMAL MAGNETOCONDUCTIVITIES OF TUNGSTEN.	25
	A. Introduction.	25
	B. Theory.	26
	1. High-Field Conductivity Tensors $\overleftrightarrow{\sigma}(H)$ and $\overleftrightarrow{w}_e(H)$	27
	2. High-Field Expressions for σ_{xx} and $(w_e)_{xx}$.	28
	3. High-Field Conductivities: Relationship to Zero-Field Resistivities and their Temperature Dependence.	37
	C. Experimental Results.	41
	D. Discussion.	48
IV	A DISCUSSION AND SOME APPLICATIONS OF HIGH-FIELD SEMICLASSICAL TRANSPORT THEORY.	56
	A. Introduction.	56
	B. The Transverse Magnetoresistance.	56
	C. The Longitudinal Magnetoresistance.	64
	D. Application of Semiclassical Transport Theory to Aspects of the Magnetoresistance of Potassium	66

Chapter		Page
V	RF SIZE EFFECT IN POTASSIUM.	71
	A. Introduction.	71
	B. The RF Size Effect.	72
	1. The Electron Trajectories	72
	2. The Electron Mean-Free Path	78
	3. Proposed Experiment	81
	C. Experimental Technique and Some Preliminary Results	82
	D. Summary	83
APPENDIX A:	Computation of the Thermal Resistivity from the Experimental Data	85
APPENDIX B:	Proof that $C_E^{(0)}(k_z, \epsilon) = (-\partial f_0/\partial \epsilon) \cdot \text{const.}$	87
APPENDIX C:	Proof that $\eta(\varphi + \pi) = -\eta(\varphi)$	89
APPENDIX D:	A Discussion of the Solution to the Zero-Field Boltzmann Equation when the Dominant Scattering Mechanism is Describable by a Relaxation Time.	91

LIST OF TABLES

Table		Page
2.1	Characteristics of the Tungsten Samples.	12

LIST OF FIGURES

Figure		Page
2.1	Diagram of cryostat.	10
2.2	Variation of the temperature-dependent part of the electrical resistivity ($\rho-\rho_o$) with T^2 for five single-crystal tungsten samples.	14
2.3	Variation of $WT-\rho_o/L_o$ with T^2 for five single-crystal tungsten samples	16
2.4	Comparison of the temperature-dependent part of the electrical resistivity ($\rho-\rho_o$) for two single-crystal tungsten samples with different crystalline orientations.	17
2.5	Comparison of $WT-\rho_o/L_o$ for two single-crystal tungsten samples with different crystalline orientations	17
2.6	Variation of the Wiedemann-Franz ratio ρ/WT with temperature for six single-crystal tungsten specimens.	18
3.1	Variation of H^2/ρ_{xx} with T^2 for various values of the magnetic field H	43
3.2	Variation of $H^2/W_{xx}T$ with temperature for several values of the magnetic field H	45
3.3	Plot of $1/W_{xx}T$ as a function of $1/H^2$ for several temperatures	46
3.4	Lattice thermal conductivity divided by temperature as a function of temperature	47
3.5	Plot of A_{xx}/T as a function of T^2.	47
4.1	Distribution functions for spherical and cubical Fermi surfaces in zero magnetic field and in a strong magnetic field.	62

Figure		Page
4.2	Distribution functions for a system with two bands.	63
5.1	Perspective drawing of a possible electron orbit in $\vec{k}$-space and the corresponding electron trajectory in real space.	76

ABSTRACT

The major part of this thesis describes a detailed study of electrical and thermal transport processes in tungsten. Chapter II is concerned with low-temperature measurements of ρ and WT (ρ is the electrical resistivity and W is the thermal resistivity) in high-purity tungsten single crystals in the absence of a magnetic field. The temperature dependence of ρ and WT is found to be predominantly quadratic, in agreement with observations in other transition metals. It is reasonable to attribute this behavior to electron-electron scattering. The validity of Matthiessen's rule for impurity and boundary scattering is investigated to determine whether the contributions of electron-electron scattering, ρ_e and W_eT, can be meaningfully separated from the total resistivities ρ and WT. In those samples in which boundary scattering contributes least to the total resistivities, Matthiessen's rule is approximately obeyed for the electrical resistivity, while deviations are observed for the thermal resistivity. For these samples, the measured values of ρ_e and W_eT yield Lorenz numbers for electron-electron scattering, $L_e = \rho_e/W_eT$, that range from 0.2×10^{-8} to 0.4×10^{-8} $W\Omega/K^2$.

Chapter III is concerned with the electrical and thermal transport properties of tungsten in a strong magnetic field. Measurements of the high-field transverse electrical and thermal conductivities, σ_{xx} and κ_{xx}, of a high-purity tungsten single crystal are presented for the temperature range 1.5 to 6 K. The magnetic field dependences of the conductivities conform excellently to the predictions of high-field semiclassical magnetoresistance theory, provided that thermal conduction by the lattice is taken into account. The results show that the lattice thermal conductivity is proportional to T^2, as expected for a pure metal in which the phonons are scattered principally by the conduction electrons. The temperature dependence of the high-

field electrical conductivity σ_{xx}, and the corresponding electronic contribution $(\kappa_e)_{xx}$ to the thermal conductivity κ_{xx} are also measured. Theoretical expresions for these quantities are derived from semi-classical magnetoresistance theory, allowing estimates to be made of the temperature dependence associated with possible low-temperature scattering mechanisms. Difficulties in interpreting the previous zero-field measurements in terms of electron-electron or electron-phonon scattering are discussed.

In Chapter IV the theory developed in Chapter III is discussed in greater detail and is extended to include a discussion of the longitudinal magnetoresistance. Next, it is shown that several interesting predictions regarding the role of electron-phonon scattering in the magnetoresistance of potassium can be made on the basis of semi-classical theory.

Lastly, in Chapter V an assessment is made of the prospect of using the rf size effect to detect anisotropies in the relaxation time in potassium.

I. INTRODUCTION

Over the past decade the Fermi surfaces of essentially all of the light metallic elements have been determined. Since the Fermi surface is important in determining the dynamics of the conduction electrons in a metal, this has led to a better understanding of many transport processes. For example, the magnetic field dependence of the high-field magnetoresistance is determined by the topology of the Fermi surface. The discovery of this fact explained the perplexing anomalies in the magnetoresistance caused by open orbits and provided a powerful tool for investigating Fermi surface topology in metals whose Fermi surfaces had not yet been determined.

However, other aspects of transport processes, such as the temperature dependence of the magnetoresistance, are determined largely by the mechanisms that scatter the conduction electrons and to a lesser extent by specific features of the Fermi surface. The study of these scattering mechanisms is the logical next step in furthering our understanding of metals.

The major part of this thesis (Chapters II and III) is concerned with the role played by low-temperature scattering mechanisms in the electrical and thermal transport properties of tungsten. At the time the measurements in zero magnetic field reported in Chapter II were completed, all the available evidence indicated that electron-electron scattering was largely responsible for the characteristic T^2 behavior of the electrical resistivity ρ and its thermal counterpart WT. However, the extension of these measurements to high magnetic fields, reported in Chapter III, has produced results that are difficult to interpret in terms of electron-electron scattering. It seems that until more is known about the role of electron-phonon scattering in the transition metals, and in particular in tungsten, it may be difficult to decide whether electron-electron or electron-phonon scatter-

ing is the dominant low-temperature scattering mechanism in tungsten; or even possibly whether it is a combination of both.

Although the role played by electron-electron scattering in the transport properties of tungsten remains ambiguous, this work has produced unexpected benefits. Firstly, the high-field measurements led to the measurement of the lattice thermal conductivity of tungsten. To my knowledge, this measurement, together with a similar independent measurement by Long, constitute the first convincing determinations of the lattice thermal conductivity of a pure metal. Secondly, some progress was made in extending high-field semiclassical theory to situations in which the scattering cannot be described by a relaxation time. Thus it is shown that, under special circumstances, the high-field electrical and thermal conductivities are given by simple expressions involving the fundamental scattering rate. Some of these results are also consequences of quantum transport theory (C. Herring, private communication). However, apart from characteristic quantum effects, such as the Shubnikov-de Haas effect, etc., the semiclassical and quantum treatments should be equivalent. Moreover, the semiclassical approach has two useful features: i) It facilitates a convenient comparison of the high-field and zero-field transport properties through the use of the Kohler variational principle; and ii) It can be modified to extend the treatment to metals having open orbits.

In Chapter IV some of the theoretical results described in Chapter III are dealt with in greater detail and have been extended in several instances. In Secs. B and C the Kohler variational principle is used to compare the high-field transverse and longitudinal magnetoresistivities. In this manner it is possible to see in a simple way the origin of the enhancement of the resistivity in a strong magnetic field. This approach seems to be naturally limited to situations for which the magnetic field is directed along a symmetry axis. It is unclear whether the same approach can be used to extend the treatment to situations

for which the magnetic field is arbitrarily oriented. Finally, in the remainder of Chapter IV some interesting predictions are made concerning the role of electron-phonon scattering the magnetoresistance of potassium.

The last chapter (Chapter V) is not directly related to any of the previous chapters. It is concerned with an assessment of the feasibility of using the rf size effect to detect anisotropies in the relaxation time in potassium.

CHAPTER II

THE LOW-TEMPERATURE ELECTRICAL AND THERMAL RESISTIVITIES OF TUNGSTEN

A. Introduction

Recently in the low-temperature electrical and thermal resistivities of several transition metals (Ni, Re, Pd, Os, Pt, and Fe)[1-7] have been measured. These studies have been important in revealing a T^2 behavior of both the electrical resistivity ρ and the analogous thermal transport property WT (W is the thermal resistivity) at low temperatures. The T^2 behavior of the electrical resistivity ρ of a number of transition metals has been known for many years[8] and was first attributed to electron-electron scattering between different branches of the Fermi surface.[9] Since that time, the observation of the T^2 behavior of WT at low temperatures in Ni, Re, Pd, Pt, and Fe has lent further support to the view that electron-electron scattering can be an important resistive mechanism in many transition metals.[10,11]

This chapter describes the extension of these measurements to tungsten. In particular, it reports a detailed study of the temperature dependence of ρ and WT in a number of high-purity tungsten single crystals for which a dominant T^2 dependence of both ρ and WT is observed in the temperature range from 1.5 to 6 K. In order to determine reliably the magnitudes of the T^2 terms in the resistivities, it was also necessary to examine the validity of Matthiessen's rule for electron-electron scattering--that is, the extent to which the coefficients of the T^2 terms in the resistivities are not affected by other scattering mechanisms such as impurity scattering and boundary scattering.

Considerable effort has been devoted to estimating theoretically the relative magnitudes of the T^2 term ρ_e in ρ and the T^2 term W_eT in WT.[12-18] Because of the difficulty of estimating the magnitudes of ρ_e and W_e separately, several calculations have been performed that give the ratio $L_e = \rho_e/W_eT$, the Lorenz number for electron-electron scattering. The first such calculation was performed by Herring[12] in

connection with the measurements of ρ_e and W_eT in nickel by White and Tainsh.[1] Herring argued that the assumption of a complicated Fermi surface could result in a considerable simplification of the collision integral for electron-electron scattering, thus making it possible to obtain an energy-dependent relaxation time. In the absence of impurity scattering this relaxation time leads to a value of L_e of 1.58×10^{-8} $W\Omega/K^2$, while for situations in which impurity scattering is predominant over electron-electron scattering, a value of 1.36×10^{-8} $W\Omega/K^2$ is obtained.[13] Although his argument does not assume any particular form for the scattering rate, Herring has noted that L_e can be quite sensitive to the angular distribution of the scattering. It is perhaps for this reason that agreement with experiment has not been particularly good. Measurements of the transport properties of Ni, Re, Pd, Pt, and Fe have yielded various values of L_e: 1.0 for Ni,[1] 0.9 for Re,[2,4] 1.1 for Pd,[3,4] 0.1 for Pt,[6] and 1.2 for Fe,[7] each in units of 10^{-8} $W\Omega/K^2$.

Other models have been considered that allow calculation of L_e for a particular scattering rate. Initial progress in this direction was made by Smith and Wilkins,[14] who found solutions to the linearized Boltzmann equation for combined electron-electron scattering and impurity scattering on a spherical Fermi surface. While this model can be expected to appropriately describe normal electron-electron scattering[15] in simple metals, it cannot be applied to the transition metals which have considerably more complicated band structures. Bennett and Rice[16] have modified this calculation to describe the scattering of mobile "s" electrons in one band by heavier "d" holes in another. To make the calculation tractable they have assumed spherical "s" and "d" bands, and, in addition, have assumed that the current is carried primarily by the "s" electrons. Although this model is still an oversimplification of the band structures of the transition metals, it is, nevertheless, instructive because it exhibits certain features

that would probabily be retained in a more realistic model. In particular their calculation shows that L_e depends rather sensitively on the angular distribution of the electron-electron scattering. In the limit of small-angle scattering, L_e approaches zero, while for isotropic scattering L_e approaches a value between 1.36×10^{-8} and 1.58×10^{-8} $W\Omega/K^2$, the exact value depending upon the amount of impurity scattering present. For intermediate angular dependences of the scattering rate, these calculations show that L_e can assume values between zero and the values calculated by Herring. Bennett and Rice point out that a scattering rate corresponding to a screened Coulomb interaction leads to values of L_e between about 0.8×10^{-8} and 1.0×10^{-8} $W\Omega/K^2$ in a typical transition metal; this is in reasonable agreement with the experimental results for Ni,[10] Re, Pd, and Fe, but not Pt. These calculations also show that significant deviations from Matthiessen's rule can occur when impurity scattering and electron-electron scattering act together. The effect is largest in the thermal resistivity, causing about a 30% increase in $[WT - (WT)_o]$ as the amount of impurity scattering is increased. In the electrical resistivity, a smaller, approximately 10% increase in $[\rho - \rho_o]$ occurs.

Other calculations have been carried out by Rice,[17] and Schriempf, Schindler, and Mills[18] using a spherical two-band model for the Fermi surface and a screened Coulomb interaction between electrons. Because a specific scattering rate is postulated, these treatments are special cases of the calculation of Bennett and Rice and lead to similar results.

To my knowledge, no measurements of the thermal resistivity of high-purity tungsten have been made in the liquid-helium temperature range. Measurements at higher temperatures in a restricted range (14-22 K) have been made by de Nobel,[19] who finds that WT can be described by $WT = (WT)_o + \beta T^3$ with $\beta \approx 5 \times 10^{-5}$ cm/WK. However, this temperature range is not sufficiently large nor the data sufficiently

precise, to distinguish between a βT^3 temperature dependence (electron-phonon scattering only) and a $\alpha T^2 + \beta T^3$ temperature dependence (electron-electron and electron-phonon scattering).

Studies of the temperature dependence of the electrical resistivity of high-purity tungsten have been made by Volkenshetyn et al.[20] and Berthel[21] over a wide range of temperatures. Volkenshetyn et al. have measured the electrical resistivity of a sample with a residual resistance ratio ($\rho(300K)/\rho(4.2K)$) of 19,000 over a temperature range extending from 4 to 300 K. They find that at low temperatures[22] the resistivity can be described by $\rho = \rho_o + AT^2 + BT^5$ with $A = 40 \times 10^{-13}$ Ω cm/K^2 and $B = 0.8 \times 10^{-15}$ Ω cm/K^5. Berthel has measured the electrical resistivity of a number of single-crystal tungsten rods with residual resistance ratios ($\rho(273K)/\rho(0K)$) ranging from 15,000 to 330,000. His measurements were made in two temperature ranges: 1.4 - 4.2 K and 14 - 27 K. In the 1.4 - 4.2 K range he finds that $\rho = \rho_o + AT^2$ with $A = 8 \times 10^{-13}$ Ω cm/K^2 in the samples which boundary scattering contributes least to the resistivity. In the samples in which boundary scattering contributes significantly to the resistivity, the coefficient A is enhanced. In the 14 - 27 K temperature range he finds that $\rho = \rho_o + C + BT^5$ with $B = 0.6 \times 10^{-15}$ Ω cm/K^5. Thus there is reasonable agreement between measurements on the magnitude of the T^5 term, but a considerable lack of agreement on the size of the T^2 term.

Berthel[21] has pointed out that in less pure samples [$\rho(273K)/\rho(0K) \leq 1500$] investigated earlier by other workers,[23,24] the temperature dependence of ρ is considerably different from that of the pure samples; in fact, the electrical resistivity does not appear to exhibit a T^5 behavior at any temperature. Qualitatively, the magnitude of the temperature-dependent part of the resistivity increases and the dependence on temperature weakens as the impurity content of the sample is increased. For example, in a polycrystalline tungsten sample with a residual resistance ratio [$\rho 295K)/\rho(0K)$] of 180, White and Woods[24]

observed at T^4 temperature dependence above 20 K and a T^2 dependence at lower temperatures. They measured a coefficient A of the T^2 term of 100 x 10^{-13} Ω cm/K^2, more than ten times larger than the coefficient measured by Berthel in high-purity single-crystal samples. The wide variation with purity of the temperature dependence of the electrical resistivity emphasizes the need to study deviations from Matthiessen's rule in experimental studies of transport processes in tungsten.

Size-effect studies in tungsten have been carried out by Berthel[25] and by Startsev et al.[26] in order to determine the electronic mean-free path. Startsev et al. have performed careful measurements on tungsten single crystals of square cross section. They reduced the thickness in small increments by more than a factor of 20 by electroetching and were especially careful to eliminate errors due to an inhomogenous distribution of impurities in the samples. Although they attempted to estimate a bulk mean-free path λ_B from their measurements by assuming a very simple model for the size effect, values of λ_B obtained in this way were not independent of sample diameter. Without a more sophisticated treatment of the dc size effect than is presently available, there is no reliable way to determine λ_B from the measured resistivity and specimen size. Roughly speaking, however, I estimate from the data of Startsev et al. that boundary scattering contributes about 60% to the resistivity of a specimen whose thickness is 1.5 mm and whose residual resistance ratio is 30,000.

B. Experimental Details

The cryostat shown in Figure 2.1 was designed so that the electrical and thermal resistivities could be measured during the same experiment.

The thermal resistivity W was determined by the usual method of measuring the temperature difference ΔT produced between two points on

the sample by a known heat current $\dot{Q}$. However, rather than computing the temperature difference directly from the measured temperatures at the two points on the sample, as is customarily done, we have used a differential technique that makes a direct comparison of the temperature along the sample with the heat current on and with it off. This technique is particularly suited to the use of small temperature differences (<30 mK), and since it is not commonly used for this type of measurement, it is useful to give a brief explanation of the method.

One end of the tungsten sample was electroplated with copper and soldered securely to a copper platform, whose temperature could be regulated electronically by means of a heater H_2 and a carbon sensing thermometer R_3. Another heater H_1, used to generate the heat current $\dot{Q}$ through the sample, was attached to the other end. In order to measure the resulting temperature difference ΔT across the sample, two carbon resistance thermometers,[27] R_1 and R_2, were soldered to copper rings electroplated to the tungsten sample about 12 cm apart. These two thermometers were connected in two arms of a Wheatstone bridge in such a way that R_1 and $\Delta R \equiv R_1-R_2$ could be measured directly. The bridge was operated at 85 Hz, and the null in the output was detected with a phase-lock amplifier. During each experiment R_1 and ΔR were calibrated against a standard germanium resistance thermometer R_4 attached to the copper platform.[28] The resistance of this thermometer was measured by means of a specially designed four-terminal bridge described elsewhere,[29] allowing measurement of the absolute temperature to an accuracy of at least 5 mK. All of the electrical leads from the sample were thermally anchored to the copper platform.

The thermal resistivity was measured as follows: first, $\Delta R(T,\Delta T) \equiv R_1(T)-R_2(T+\Delta T)$ and $R_1(T)$ were measured with a heat current $\dot{Q}$ flowing in the sample. Next the heat current was reduced to zero and the temperature of the platform was adjusted by means of the regulator to keep R_1 at the same temperature, and then $\Delta R(T,0) = R_1(T)-R_2(T)$ was measured. The temperature difference ΔT was calculated by the expression

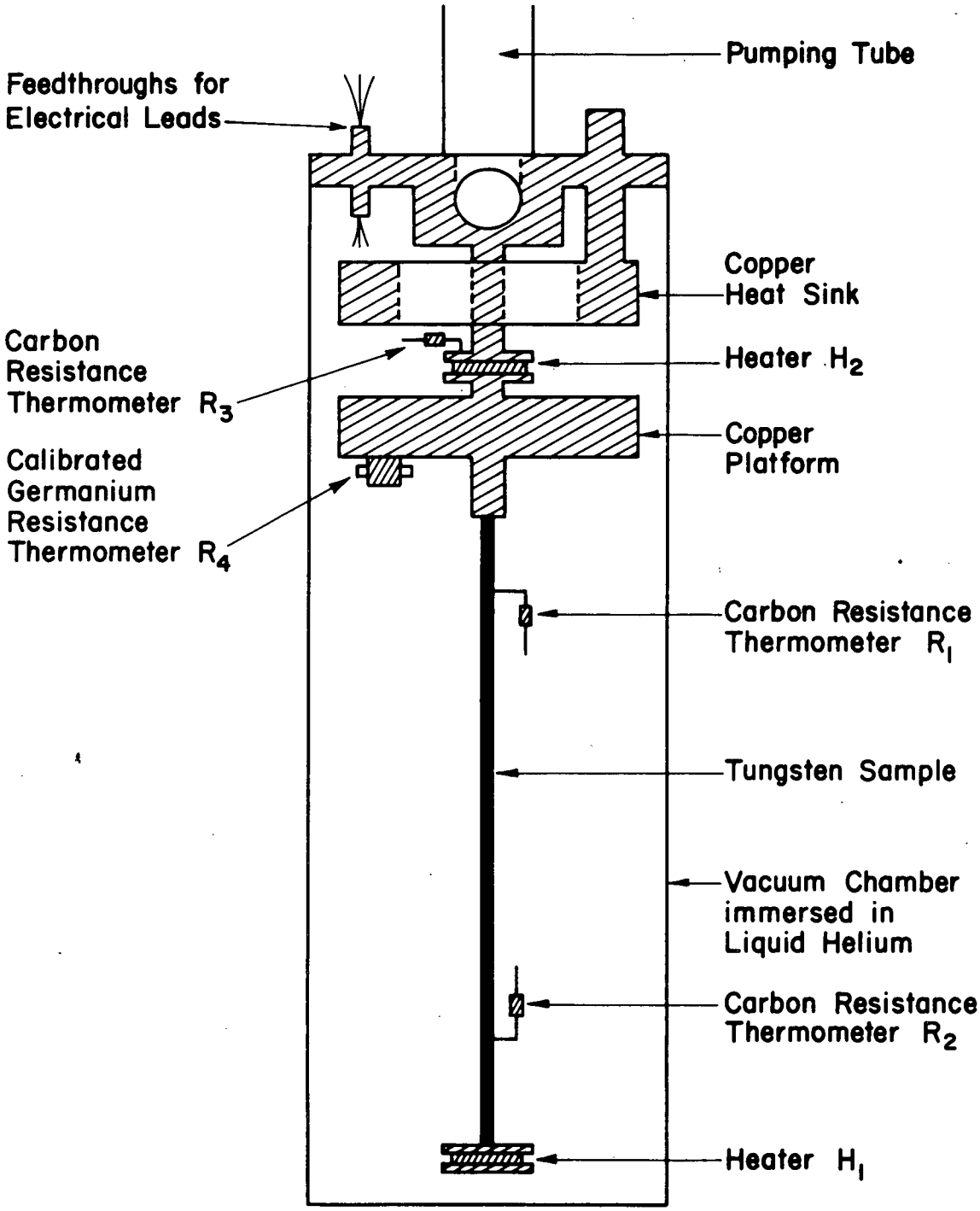

Figure 2.1. Diagram of the cryostat. Electrical leads are brought into the vacuum chamber via Epoxy feedthroughs and are anchored thermally to the heat sink. From the heat sink, short constantan wires run to the copper platform where they are again thermally anchored. From the platform, connections are made to the sample.

$$\Delta T = - \frac{\Delta R(T, \Delta T) - \Delta R(T, 0)}{dR_2/dT} \qquad (2\cdot1)$$

which is valid provided $|dR_2/dT| >> \frac{1}{2}|d^2R_2/dT^2|(\Delta T)$ (see Appendix A). Finally, the thermal resistivity W was calculated from $W = (\Delta T/\dot{Q})(A/L)$, where A/L is the ratio of the cross-sectional area A of the specimen and the distance L between the copper rings. This ratio was determined by measuring the resistance of the sample at room temperature, using a value of 5.38 $\mu\Omega$ cm for the room temperature resistivity to compute A/L; in computing this ratio I have neglected the small change that occurs due to contraction as the sample is cooled to liquid helium temperature. It was verified that the thermal resistivity W was independent of the heat current used for a tenfold change in heat current and it was possible to measure W with a precision of about 1% for the samples with diameters of 1.5 mm or smaller, and with a precision of about 8% for the 3.0 mm samples. The peak in the thermal conductivity of each of the samples occurred at about 4K, and in the purest specimen the peak value was 750 W/cm K (the room-temperature thermal conductivity of tungsten is 1.3 W/cm K). The samples, their diameters, and other pertinent characteristics are listed in Table 2.1.

The electrical resistivity was measured in the customary four-probe manner. Two fine-copper voltage leads were attached to the sample at the points where the thermometers were attached, and a superconducting wire was used as the current lead. A constant current was passed through the sample, and the potential produced between the voltage leads was measured by a Keithley 148 nanovoltmeter with an integrating digital voltmeter readout. A current of 2A was used in the 1.0- and 1.5-mm-diameter samples and 4A was used in the 3.0-mm-diameter samples. By making measurements at different currents it was verified that there were no measurable deviations from Ohm's law at these current levels due to the large magnetoresistance of tungsten. In these

Table 2.1 Characteristics of the Tungsten Samples

Sample*	Surface Condition	Diameter (mm)	r_R	r_R/d (mm^{-1})	ρ_o ($10^{-10}\Omega cm$)	$(WT)_o$ ($10^{-2}K^2cm/W$)
W-2	mirror	1.5	59,000	39,000	0.912±.002	0.386±.004
W-3	mirror	1.5	43,000	29,000	1.231±.004	0.491±.004
W-4	matt	1.0	30,000	30,000	1.780±.004	0.721±.005
W-5	matt	1.5	9,400	6,300	5.724±.006	2.266±.014
W-6	mirror	3.0	63,000	21,000	0.848±.012	0.316±.010
W-7	mirror	3.0	95,000	32,000	0.566±.004	0.214±.010
W-8	mirror	1.5	75,000	50,000	0.695±.006	0.319±.002
W-8A	matt	0.8	31,000	40,000	1.748±.006	0.717±.004
W-8B	matt	1.5	53,000	35,000	1.006±.012	0.426±.006

Sample	A ($10^{-13}\Omega cm/K^2$)	B ($10^{-15}\Omega cm/K^5$)	α ($10^{-4}cm/W$)	$L_e = A/\alpha$ ($10^{-8}W\Omega/K^2$)	$\rho_o(WT)_o$ ($10^{-8}W\Omega/K^2$)
W-2	6.8 ± 0.3	1.1 ± 0.1	----------	----------	2.36 ± .03
W-3	7.2 ± 0.5	1.6 ± 0.2	2.51 ± .02	0.29 ± .06	2.51 ± .02
W-4	7.4 ± 0.4	1.5 ± 0.2	2.55 ± .03	0.29 ± .02	2.47 ± .02
W-5	6.2 ± 0.6	1.8 ± 0.3	2.91 ± .08	0.21 ± .02	2.53 ± .02
W-6	6.7 ± 1.1	1.3 ± 0.4	2.21 ± .08	0.30 ± .05	2.68 ± .08
W-7	8.7 ± 0.3	0.8 ± 0.1	2.17 ± .06	0.40 ± .02	2.64 ± .11
W-8	11.0 ± 0.6	1.3 ± 0.3	2.53 ± .01	(0.44±.02)	2.18 ± .02
W-8A	12.2 ± 0.6	0.7 ± 0.3	2.78 ± .02	(0.44±.02)	2.44 ± .01
W-8B	9.7 ± 1.4	1.0 ± 0.6	2.48 ± .03	(0.39±.06)	2.36 ± .03

*All samples have a [110] axis oriented along the rod axis except W-2 which has a [111] orientation.

The errors shown represent 95% confidence limits (two standard deviations) calculated from the rms deviation of the data from the fit.

samples the resistivity ρ could be measured to a relative precision of about $\frac{1}{2}\%$. An exception occurred in the sample with the smallest diameter (sample W-8A). In this sample a resistance that decreased slightly with measuring current was observed. Consequently a current of 1A was used to minimize this effect, thereby incurring an error of at most 2%.

Considerable care was taken to eliminate two potential sources of systematic error in the thermal measurements: (i) loss of heat from the sample via the electrical leads, and (ii) loss of heat from the sample via conduction by residual helium gas in the vacuum chamber surrounding the sample. In the first case, the loss of heat through the constantan heater and the thermometer wires was negligible. To verify that there was no significant heat loss through the copper voltage leads and the superconducting current lead, these wires were disconnected and the thermal resistivity was remeasured for two samples W-3 and W-7. In each case the measurements produced results completely consistent with the original measurements made with the wires in place. It was also verified that conduction through the vacuum space was negligible by changing the temperature between the walls of the chamber and the sample; in addition, an adsorbent[30] was placed in the vacuum chamber to adsorb residual helium gas.

C. Experimental Results

The resistivities of seven electron-beam zone-refined single-crystal tungsten specimens were measured. Six were oriented with the [110] direction parallel to the rod axis, and one was oriented with the [111] direction parallel to the rod axis (see Table 2.1).

In Figure 2.2 the temperature-dependent part of the electrical resistivity ($\rho - \rho_0$) has been plotted as a function of the square of the temperature for five tungsten specimens of various diameters and purities, each oriented with the [110] direction parallel to the rod axis. The most notable feature of Figure 2.2 is the large temperature

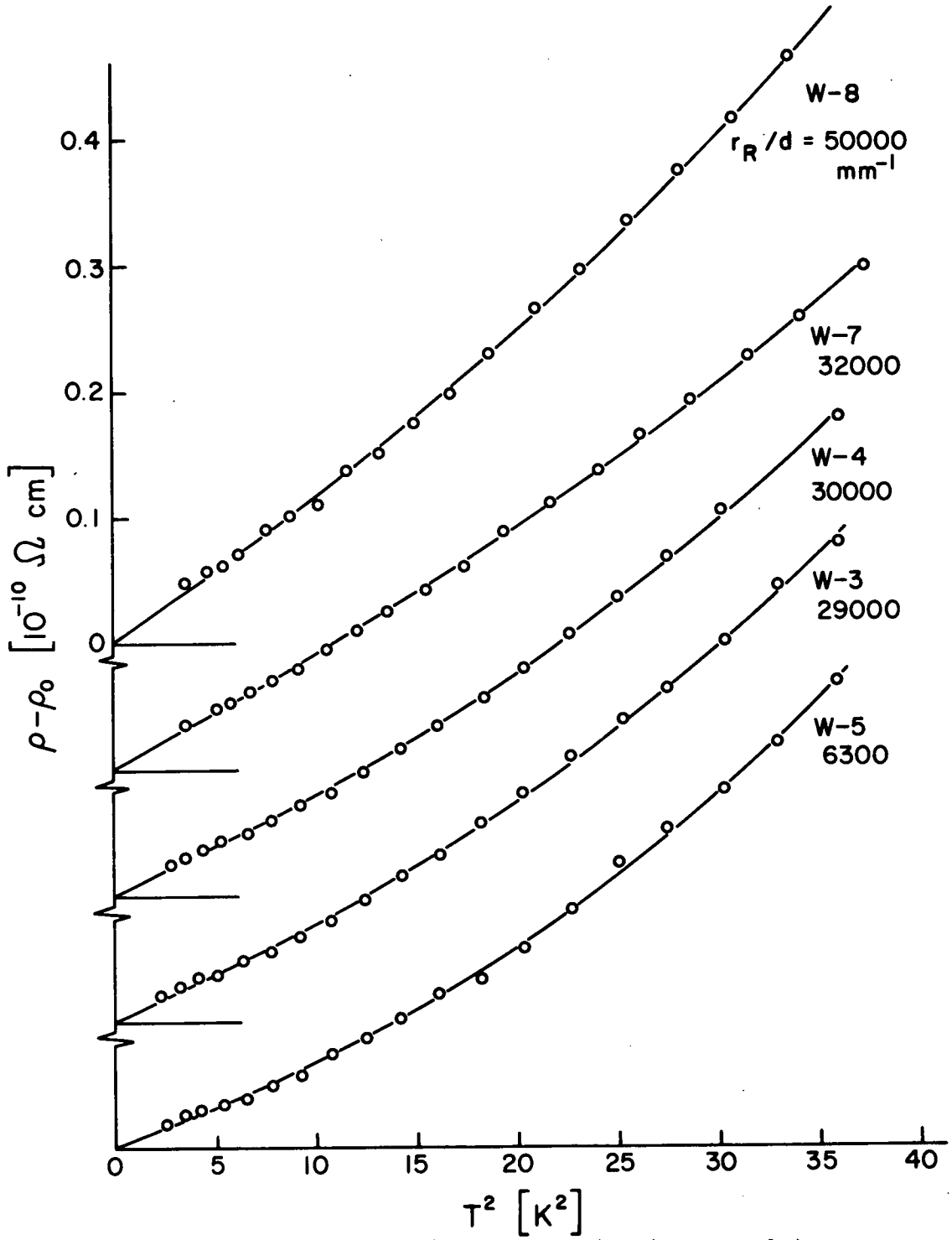

Figure 2.2. Variation of the temperature-dependent part of the electrical resistivity ($\rho - \rho_0$) with T_2 for five single-crystal tungsten samples, each oriented with the [110] direction parallel to the rod axis. The origin of each plot has been displaced vertically for clarity and the plots have been arranged in order of r_R/d. Each of the solid curves represents a function of the form $AT^2 + BT^5$, determined by the method of least squares.

dependence of the resistivity for sample W-8 compared to the other samples. Similar results have been reported by Berthel,[21] who shows convincingly that this is due to the size effect. Following the treatment of Berthel, I have used the parameter r_R/d to characterize the relative amount of boundary scattering in the samples [where r_R stands for the residual resistance ratio, $\rho(299K)/\rho(0K)$, of a specimen diameter d]. Except in the extreme size-effect regime (where r_R/d tends to a constant value) the parameter r_R/d can be expected to increase roughly with increasing boundary scattering. As expected, sample W-8 has the largest value of r_R/d, while sample W-7--which does not show an enhancement of the temperature dependent resistivity--has the largest residual resistance ratio.

The temperature dependence of the electrical resistivity of all of the samples can be adequately described by $\rho = \rho_o + AT^2 + BT^5$ for the temperature range covered in this experiment. For those samples in which Matthiessen's rule is approximately obeyed, it is reasonable to identify each of these terms with the unique contributions of impurity and boundary scattering, electron-electron scattering, and electron-phonon scattering. Although the real situation may be more complicated, there does not exist at present a more soundly based expression having as few parameters; consequently I have been obliged to use this expression to fit the data. The values of ρ_o, A, and B were determined by the method of least-squares for each of the samples and tabulated in Table 2.1.

In Figure 2.3 the variation of WT with T^2 is shown for each of the five tungsten samples shown in Figure 2.2. The temperature dependence of WT can be described by $WT = (WT)_o + \alpha T^2$. A βT^3 term in WT, corresponding to the BT^5 term in ρ due to electron-phonon scattering is not evident in the data; if such a term is present, the coefficient β would have to be smaller than 5×10^{-6} cm/WK. As shown in Table 2.1, the value of α varies by about 30% among the samples oriented with the

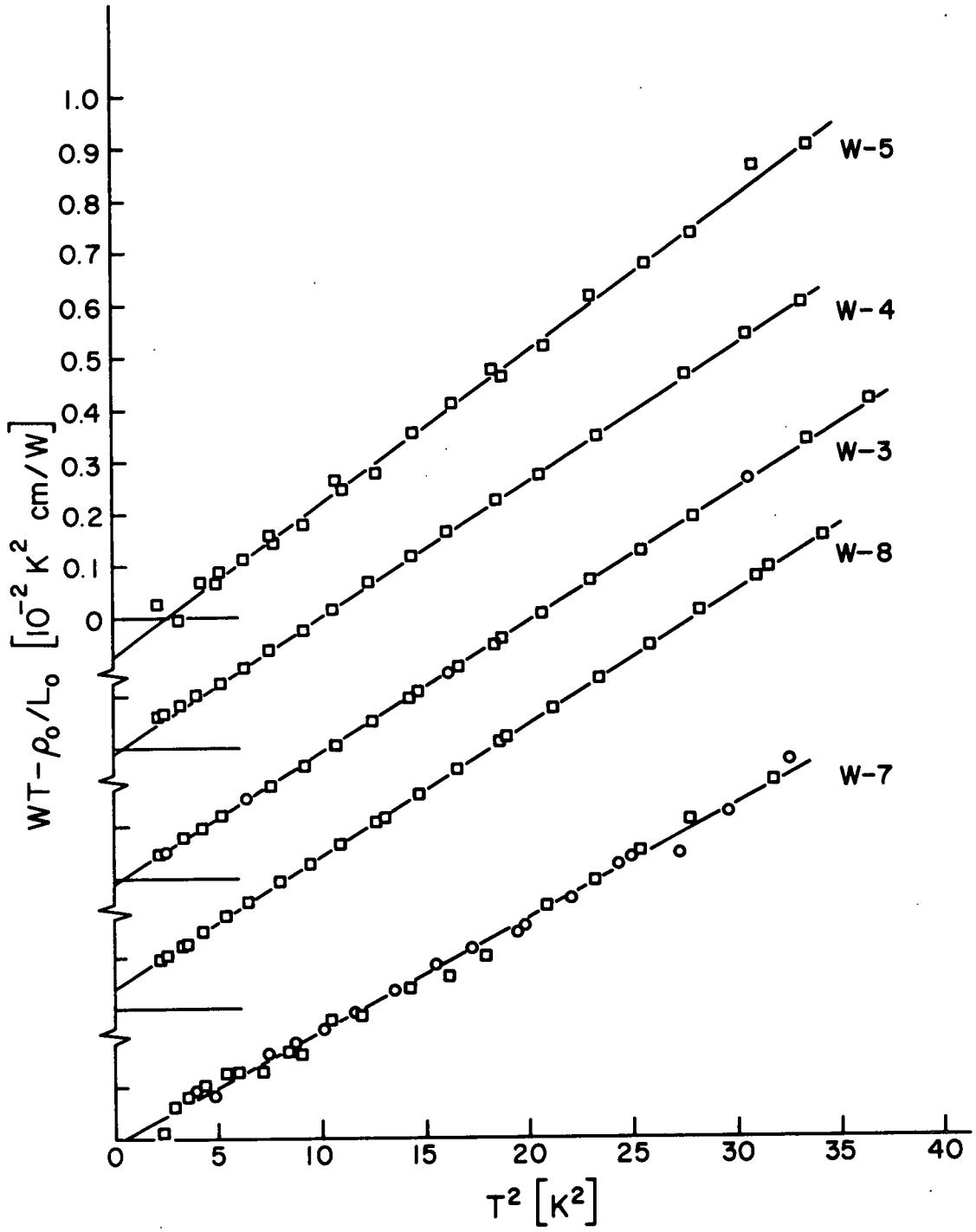

Figure 2.3 Variation of $WT - \rho_0/L_0$ with T^2 for five single-crystal tungsten samples, each oriented with the [110] direction parallel to the rod axis. The origin of each plot has been displaced vertically for clarity and the plots have been arranged in order of r_R. Square data points were taken with the potential leads and current lead attached to the sample, while the circled points were taken in a separate experiment with these leads disconnected.

[110] direction along the rod axis. In general, the value of α tends to increase with increasing impurity content, although sample W-8 appears again to be an exception.

These measurements were performed mainly on specimens with the [110] direction parallel to the rod axis; however, one specimen W-2 with the [111] direction parallel to the rod axis was also studied. In Figures 2.4 and 2.5, the resistivities of samples W-2 and W-3 are compared. Although the temperature dependences of the electrical resistivities for the two samples are nearly identical, the temperature dependences of the thermal resistivities are qualtitatively different; sample W-3 appears to exhibit a quadratic temperature variation whereas sample W-2 increases at a slightly faster rate. Ordinarily, in bulk material the resistivities of a cubic crystal, such as tungsten, must be isotropic due to the symmetry of the lattice. However, in specimens with significant amounts of boundary scattering, exceptions can be expected to occur.[31]

In Figure 2.6 the variation of the Wiedemann-Franz ratio ρ/WT with temperature is shown for the six samples plotted in Figures 2.2-2.5. The Wiedemann-Franz ratios of the samples in which boundary scattering is not appreciable (W-3, W-4, W-5, and W-7) extrapolate to within a few percent of the Lorenz number $L_o = 2.44 \times 10^{-8}$ WΩ/K^2 as the temperature approaches absolute zero. This behavior is expected when the scattering is dominated by elastic impurity scattering.[32] On the other hand, sample W-8, for which boundary scattering is expected to be appreciable, shows a departure from the Wiedemann-Franz law that is many times larger than the limits set by the random error in the experiment.

Further measurements on sample W-8 were performed in an attempt to clarify this effect. Sample W-8 was spark cut into two shorter rods of equal length. The residual resistance ratio of each half was measured and was found to be essentially the same as that of the original sample. One side of one of the pieces was removed by electro-

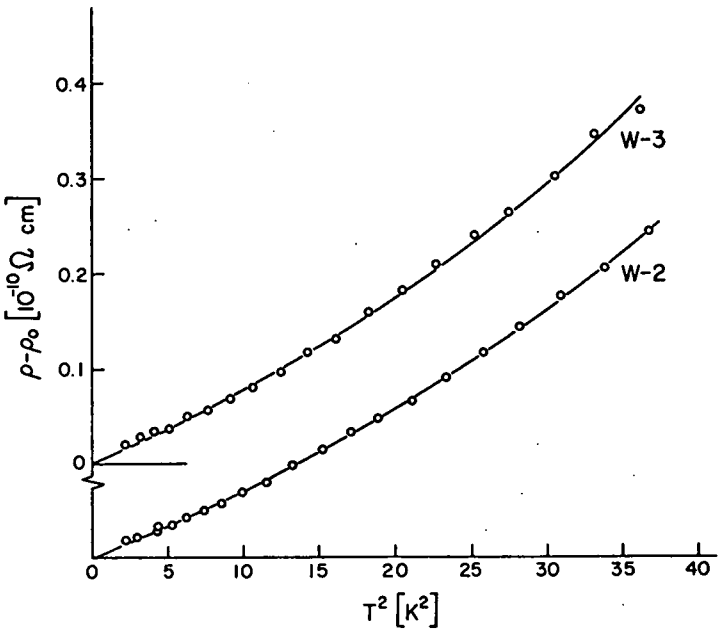

Figure 2.4. Comparison of the temperature-dependent part of the electrical resistivity ($\rho - \rho_0$) for two single-crystal tungsten samples with different crystalline orientations. Samples W-2 and W-3 were oriented with the [111] and [110] directions parallel to the rod axis.

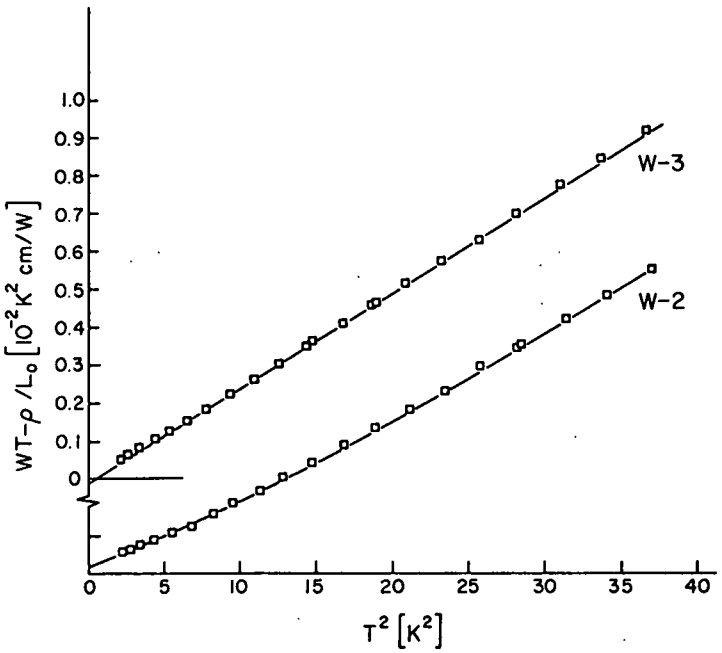

Figure 2.5. Comparison of WT - ρ_0/L_0 for two single-crystal tungsten samples with different crystalline orientations. Samples W-2 and W-3 were oriented with the [111] and [110] directions parallel to the rod axis, respectively.

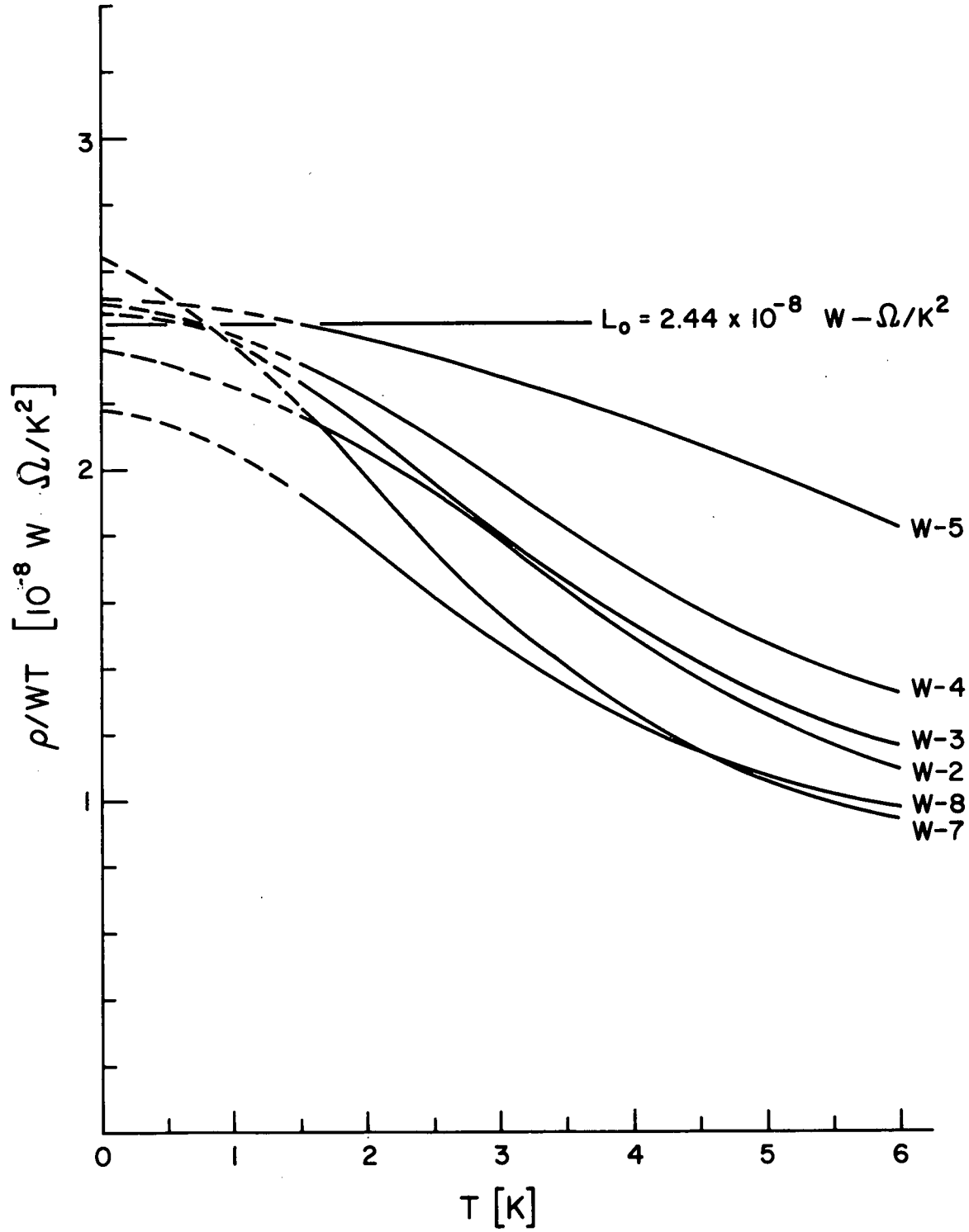

Figure 2.6. Variation of the Wiedemann-Franz ratio ρ/WT with temperature for six single-crystal tungsten specimens.

etching to produce a specimen with a smaller effective diameter (semi-circular cross section) but with substantially the same mean impurity content. This sample was designated W-8A. The other piece was electro-etched uniformly for a short period to remove the mirror finish of sample W-8, resulting in a sample with a matt finish identical to that of W-8A, but with a diameter essentially the same as sample W-8. This sample was designated W-8B.

The results of measurements of the resistivities of these two samples are shown in Table 2.1. Most noteworthy are two facts: (i) The Wiedemann-Franz ratio of each sample extrapolates to within a few percent of the Lorenz number as the temperature approaches absolute zero, and (ii) The residual resistance ratio of sample W-8B is 53,000--significantly smaller than the 75,000 residual resistance ratio of sample W-8. A further brief etching of the surface reduced the residual resistance ratio of sample W-8B to only 49,000. These results indicate that the nature of the sample surface may be important in determining the contribution of boundary scattering to the resistivity. It is interesting to conjecture that specular scattering may be responsible for these effects. Although this could explain the sharp decrease in the residual resistance ratio of sample W-8B after the removal of the mirror finish, it is not clear why the Wiedemann-Franz ratio should also be affected. Further experiments as well as a better characterization of the smoothness of the sample surface would help clarify the puzzling behavior of this sample.

From the values of A and α determined from the electrical and thermal resistivity measurements, I have calculated the Lorenz number for electron-electron scattering, $L_e = A/\alpha$, as shown in Table 2.1. This ratio is probably not very meaningful for samples W-8, W-8A, and W-8B because of the size-effect enhancement of A. For the other samples, L_e ranges between 0.2×10^{-8} and 0.4×10^{-8} $W\Omega/K^2$.

D. Discussion

A central problem in this investigation has been the separation and identification of the scattering processes important in tungsten at low temperatures. In order to identify each scattering mechanism from the temperature dependence of the resistivity, I felt that it was necessary to perform measurements on enough samples to be able to assess the validity of Matthiessen's rule. The purity of the tungsten samples that were used covered a tenfold range from 9,400 to 95,000. The results indicate that the magnitude of the T^2 term in ρ is not substantially affected by the presence of impurity scattering. On the other hand, with the exception of sample W-8 for which boundary scattering is appreciable, the magnitude of the T^2 term in WT appears to increase systematically with increasing impurity content. These observations are in qualitative agreement with the theoretical calculation of Bennett and Rice.[16]

I have also tried to assess the effect of boundary scattering on the temperature dependence of the resistivities. The temperature dependence of the electrical resistivity is not appreciably affected by the presence of boundary scattering in those samples for which $r_R/d < 30{,}000\ mm^{-1}$. However, for greater values of r_R/d, the temperature dependence is enhanced. If a similar effect occurs for WT it is clear that it is comparable to or smaller than the deviations from Matthiessen's rule that are ascribed to impurity scattering.

These data, and especially those of Volkenshteyn[20] and Berthel[21] which extend to higher temperatures, show an apparent T^5 behavior of ρ in high purity samples which is presumably a consequence of electron-phonon scattering. However, I have found no indication of a corresponding T^3 term in WT. At low temperatures electron-phonon scattering is confined to small angles and is inelastic, so that the Wiedemann-Franz ratio for this type of scattering should be substantially smaller than L_o, i.e., $BT^5/\beta T^3 \ll L_o$, or equivalently $\beta \gg BT^2/L_o$. Using the

measured values of B, I estimate that at 6 K, $\beta >> 2 \times 10^{-6}$ cm/WK. Although a value as small as 5×10^{-6} cm/WK should be observable, I have been unable to detect any T^3 variation in WT at all.

The principal evidence for the presence of electron-electron scattering in the transition metals is the dominant T^2 dependence of both ρ and WT at low temperatures.[33] To the extent that it is possible to isolate the contribution of electron-electron scattering to the total resistivities, I have calculated the Lorenz number for electron-electron scattering in tungsten and have obtained values ranging from 0.2×10^{-8} to 0.4×10^{-8} $W\Omega/K^2$ for samples W-3, W-4, W-5, W-6, and W-7. These values are significantly below the values calculated by Herring, yet are consistent with the calculation of Bennett and Rice,[16] which does allow lower values for L_e. However, it is doubtful that quantitative agreement with these theories should be expected in tungsten in view of the obvious shortcomings of the two-band model for this metal. Considerable s-d hybridization of the electron wavefunctions occurs in tungsten, making the distinction between s and d portions of the Fermi surface much less meaningful in tungsten than, for example, in palladium. It may be significant, however, that the theories do allow a decrease in L_e below the Herring values in accord with all the experimental results obtained to date.

REFERENCES

1. G. K. White and R. J. Tainsh, Phys. Rev. Letters 19, 165 (1967).
2. J. T. Schriempf, J. Phys. Chem. Solids 28, 2581 (1967).
3. J. T. Schriempf, Phys. Rev. Letters 19, 1131 (1967).
4. J. T. Schriempf, Phys. Rev. Letters 20, 1034 (1968).
5. J. T. Schriempf, Solid State Comm. 6, 873 (1968).
6. A. C. Anderson, R. E. Peterson, and J. E. Robichaux, Phys. Rev. Letters 20, 459 (1968).
7. J. G. Beitchman, C. W. Trussel, and R. V. Coleman, Phys. Rev. Letters 25, 1291 (1970).
8. See for example, W. J. de Haas and J. de Boer, Physica 1, 609 (1933) and G. K. White and S. B. Woods, Phil. Trans. Roy. Soc. London A251, 273 (1959).
9. W. G. Baber, Proc. Roy. Soc. London A158, 383 (1937); for a general discussion of electron-electron scattering see N. F. Mott, Adv. Phys. 13, 405 (1964).
10. There has been some controversy over the interpretation of the results of Ref. 1; see F. C. Schwerer and J. Silcox, Phys. Rev. Letters 20, 101 (1968) and A. Fert and I. A. Campbell, Phys. Rev. Letters 21, 1190 (1968).
11. In Os the T^2 term in WT was obscured by electron-phonon scattering which contributes a T^3 term to WT.
12. C. Herring, Phys. Rev. Letters 19, 167 (1967); 19, 684(E) (1967).
13. C. Herring, private communication.
14. H. Smith and J. W. Wilkins, Phys. Rev. 183, 624 (1969).
15. Umklapp processes are not explicitly considered; in their absence the contribution of normal electron-electron scattering to the electrical resistivity vanishes.
16. A. J. Bennett and M. J. Rice, Phys. Rev. 185, 968 (1969).
17. M. J. Rice, Phys. Rev. Letters 20, 1439 (1968).

18. J. T. Schriempf, A. I. Schindler, and D. L. Mills, Phys. Rev. 187, 959 (1969). Although this paper deals with Pd:Ni alloys in the context of electron-paramagnon scattering, a brief discussion of electron-electron scattering in Pd and Re is given on pages 971-2.

19. J. de Nobel, Physica 23, 349 (1957).

20. N. V. Volkenshteyn, L. S. Starostina, V. Ye. Startsev, and Ye. P. Romanov, Fiz. Metal. i Metalloved. 18, 888 (1964) [Phys. Metals Metallog. (USSR) 18, 85 (1964)].

21. K. H. Berthel, Phys. Stat. Sol. 5, 399 (1964).

22. By low temperatures it is meant temperatures for which $\rho_0 > \frac{1}{2}(\rho - \rho_0)$. The coefficient in T^2 quoted in the translation of Ref. 20 is in error; the value quoted in the original article is smaller by a factor of ten.

23. G. J. van den Berg, Physica 14, 111 (1948).

24. G. K. White and S. B. Woods, Canad. J. Phys. 35, 656 (1957).

25. K. H. Berthel, Phys. Stat. Sol. 5, 159 (1964).

26. V. Ye. Startsev, N. V. Volkenshteyn, and G. Q. Nikitina, Fiz. Metal. i Metalloved. 26, 261 (1968) [Phys. Metals Metallog. (USSR) 26, 76 (1968)].

27. 56 ohm, 1/10 watt, Allen Bradley Co., Milwaukee, Wisconsin. The resistors used were matched to about 1% at 4.2K.

28. CR2500L, Cryocal Inc., Riviera Beach, Florida.

29. J. W. Ekin and D. K. Wagner, Rev. Sci. Instr. 41, 1109 (1970).

30. Molecular sieve, Union Carbide International Co., Division of Union Carbide Corporation, New York, N. Y.

31. See for example, The Physics of Metals I. Electrons, edited by J. M. Ziman, (Cambridge University Press, Cambridge, 1969) p. 185-9.

32. G. V. Chester and A. Thellung, Proc. Roy. Soc. 77, 1005 (1961).

33. New independent evidence for electron-electron scattering has been obtained in field emission studies of tungsten at 20K;

C. Lea and R. Gomer, Phys. Rev. Letters 25, 804 (1970).

34. J. R. Clement and E. H. Quinell, Rev. Sci. Instr. 23, 213 (1952).

CHAPTER III

THE LATTICE THERMAL CONDUCTIVITY AND HIGH-FIELD ELECTRICAL AND THERMAL MAGNETOCONDUCTIVITIES OF TUNGSTEN

A. Introduction

In the previous Chapter I described measurements of the low-temperature electrical and thermal resistivities of tungsten in the absence of a magnetic field.[1] Like many other transition metals, ρ and WT (ρ and W are the electrical and thermal resistivites, respectively) exhibit a predominantly T^2 dependence at low temperatures, suggesting that the dominant low-temperature scattering mechanism is electron-electron scattering. However, only a small amount of independent evidence exists to support this interpretation.[2] Therefore, it was felt that it would be useful to investigate the temperature dependence of the electrical and thermal conductivities of tungsten in a strong magnetic field to provide further information about the low-temperature scattering mechanisms.

In this chapter measurements are presented of the transverse electrical and thermal conductivities, σ_{xx} and κ_{xx}, of a high-purity tungsten crystal, oriented with the magnetic field along the [001] direction. The measurements span a range of temperature from 1.5 to 6 K and a range of magnetic field strength from 2.7 to 18.6 kG. Extensive use of high-field semiclassical magnetoresistance theory[3-5] is made to separate the lattice and electronic components κ_g and $(\kappa_e)_{xx}$ from the total thermal conductivity κ_{xx}, and to interpret the temperature dependences of the electronic conductivities σ_{xx} and $(\kappa_e)_{xx}$ at high fields.

To provide the framework for analyzing these measurements the relevant aspects of the high-field theory are presented in Sec. B. In Sec. B1 the magnetic field dependence of the conductivities predicted by the high-field theory is summarized. As shown by Lifshitz, Azbel, and Kaganov (LAK),[3,4] these results reflect the topology of the

Fermi surface and do not depend upon the nature of the scattering mechanism. In Secs. B2 and B3 the LAK treatment is reviewed and extended to investigate the temperature dependence of σ_{xx} and $(\kappa_e)_{xx}$, which, unlike the magnetic field dependence, is determined by the scattering mechanisms. In particular it is shown that at high fields, with the magnetic field directed along a high-symmetry axis, each scattering mechanism contributes in a strictly additive fashion to σ_{xx} and $(\kappa_e)_{xx}$. In this respect, high-field measurements of σ_{xx} and $(\kappa_e)_{xx}$ should be less ambiguous than zero-field measurements of ρ and W, for which the additivity of the contributions of different scattering mechanisms (Matthiessen's rule) is only approximate. In addition, simple expressions for the contributions of various scattering mechanisms to σ_{xx} and $(\kappa_e)_{xx}$ are derived, allowing estimates of the temperature dependence of each contribution to be made. In Sec. C the experimental results are presented, and this is followed by a discussion of these results in Sec. D. Difficulties in interpreting both the previous zero-field results and the present high-field results in a consistent manner in terms of electron-electron or electron-phonon scattering are discussed. Lastly, a comparison of the results reported in this paper with similar recent measurements in tungsten by Long is made.

B. Theory

Section B1 consists of a general consideration of the magnetic field dependence of the high-field electrical and thermal conductivity tensors, $\overleftrightarrow{\sigma}(H)$ and $\overleftrightarrow{\kappa}_e(H)$. The discussion is specialized to those cases in which the magnetic field $\vec{H}$ is oriented along a high-symmetry direction (threefold, fourfold, or sixfold symmetry axis), and to metals, such as tungsten, in which the sheets of the Fermi surface are closed. It should be emphasized that these results are applicable to any scattering mechanism and do not depend upon the existence of a relaxation time. In Sec. B2 the explicit dependence of the conductivity tensor

elements σ_{xx} and $(\kappa_e)_{xx}$ upon the nature of the scattering mechanism is considered. Finally in Sec. B3, the relationship of the high-field conductivities to the zero-field resistivities is explored, and estimates of the temperature dependences of the high-field conductivities are made for several scattering mechanisms.

1. High-Field Conductivity Tensors $\overleftrightarrow{\sigma}(H)$ and $\overleftrightarrow{\kappa}_e(H)$

It is simplest to discuss first the field dependence of the electrical conductivity tensor $\overleftrightarrow{\sigma}(H)$. With the magnetic field along a high-symmetry direction, the conductivity tensor $\overleftrightarrow{\sigma}(H)$ assumes the simple form: $\sigma_{xx}(H) = \sigma_{yy}(H)$, $\sigma_{yx}(H) = -\sigma_{xy}(H)$, and $\sigma_{xz}(H) = \sigma_{zx}(H) = \sigma_{yz}(H) = \sigma_{zy}(H) = 0$. These relations, coupled with the Onsager relation $\sigma_{ij}(H)$ and $\sigma_{ji}(-H)$ require that $\sigma_{xx}(H)$ and $\sigma_{xy}(H)$ be even and odd functions of H, respectively. According to semiclassical magnetoresistance theory,[3] if the Fermi surface is closed, the tensor elements σ_{xx} and σ_{xy} have the following asymptotic form at high fields:[6] $\sigma_{xx} \sim a_{xx}(T)/H^2$ and $\sigma_{xy} \sim (n_e - n_h)ec/H + a_{xy}(T)/H^3$, where n_e and n_h are the number of electrons and holes, respectively, and $a_{xx}(T)$ and $a_{xy}(T)$ are generally temperature-dependent quantities that depend upon the nature of the scattering processes in the metal. Since tungsten is compensated ($n_e = n_h$), it follows that $\sigma_{xy} \sim a_{xy}(T)/H^3$. At high fields, inversion of the conductivity tensor gives:

$$\frac{1}{\rho_{xx}} \sim \sigma_{xx} \sim \frac{a_{xx}(T)}{H^2} , \qquad (3\cdot1)$$

where $\overleftrightarrow{\rho}(H)$ is the electrical resistivity tensor. Equation (3·1) is valid at fields strong enough such that $|a_{xx}H/a_{xy}|^2 >> 1$, or in terms of directly measurable quantities $|\rho_{xx}|^2 >> |\rho_{xy}|^2$.

The thermal conductivity tensor $\overleftrightarrow{\kappa}_e(H)$ can be treated in a similar manner.[4,7] At high fields the tensor elements $(\kappa_e)_{xx}$ and $(\kappa_e)_{xy}$ have the following asymptotic form: $(\kappa_e)_{xx} \sim A_{xx}(T)/H^2$ and

$(\kappa_e)_{xy} \sim L_0 T(n_e - n_h)ec/H + A_{xy}(T)/H^3$, where $L_0 = 2.44 \times 10^{-8}$ WΩ/K^2 is the Lorenz number, and $A_{xx}(T)$ and $A_{xy}(T)$ are generally temperature-dependent quantities that depend upon the nature of the scattering processes in the metal. These quantities and their electrical counterparts obey the Wiedemann-Franz law if the scattering is elastic; that is, $A_{xx}/Ta_{xx} = L_0$ and $A_{xy}/Ta_{xy} = L_0$. If the scattering is not elastic, these ratios will generally be larger than the Lorenz number L_0.

At this point only thermal conduction by the electrons has been considered. In fact, some heat is conducted by the phonons (lattice) in addition to that conducted by the electrons. Assuming that the two conduction mechanisms are independent, the conductivity tensors for electron and phonon conduction simply add to give the total conductivity tensor $\overleftrightarrow{\kappa}(H)$. Thus, at high fields in a compensated metal, we have $\kappa_{xx} \sim \kappa_g(T) + A_{xx}(T)/H^2$ and $\kappa_{xy} \sim A_{xy}(T)/H^3$, where κ_g is the thermal conductivity of the lattice. Letting $\overleftrightarrow{W}(H)$ be the thermal resistivity tensor,[8] inversion of the thermal conductivity tensor at high fields gives

$$\frac{1}{W_{xx}T} \sim \frac{\kappa_{xx}}{T} \sim \frac{\kappa_g}{T} + \left(\frac{A_{xx}(T)}{T}\right)/H^2 \ . \qquad (3\cdot2)$$

Expressions for $a_{xx}(T)$ in Eq. (3·1) and $A_{xx}(T)/T$ in Eq. (3·2) are derived in Sec. B2, showing the explicit dependence of these two quantities upon the scattering mechanism.

2. High-Field Expressions for σ_{xx} and $(\kappa_e)_{xx}$

In a metal with several valence electrons, portions of the Fermi surface will generally be distributed among one or more bands and will therefore occupy one or more Brillouin zones. The portion of the Fermi surface belonging to a single band may consist of one or more surfaces or sheets, which we assume to be closed. In the presence of a magnetic field $\vec{H}$ along the z axis, an electron on one of these sheets will move on the orbit formed by the intersection of this sheet with a

plane perpendicular to the magnetic field. Following the semiclassical theory of LAK, the motion of the electron in $\vec{k}$-space can be described in terms of its component of wave vector k_z along the magnetic field, its energy ϵ, and a coordinate φ that measures its position on the orbit. For a given orbit (specified by k_z and ϵ) φ is defined by

$$\varphi = -\omega_c \frac{\hbar c}{eH} \int \frac{dk_\parallel}{v_\perp} , \tag{3.3}$$

calculated from an arbitrary point on the orbit. In this expression, $dk_\parallel$ is an element of arc along the orbit taken in the direction of motion, and $v_\perp$ is the component of velocity perpendicular to the magnetic field. ($v_\perp$ is taken to be positive if directed outward from the orbit.) The cyclotron frequency ω_c is defined such that one full orbit corresponds to a change of φ by 2π. In general, ω_c will have a different value for each orbit and will be therefore a function of k_z and ϵ.

In the semiclassical theory, the electric and magnetic fields are assumed not to cause interband transitions,[9] but interband scattering is allowed. However, because the inclusion of interband scattering into the theory only complicates the formalism without altering the principal results, we shall consider initially only intraband scattering in this section. Thus each band can be treated independently. For simplicity we assume that the band under consideration contains only a single sheet of the Fermi surface. Finally, at the end of this section we discuss the results that are obtained when these restrictions are relaxed.

In the presence of an electric field $\vec{E}$ along the x axis in addition to the magnetic field $\vec{H}$ along the z axis, the steady state distribution function f will deviate by an amount $eE_x\eta_E$ from its value f_0 at equilibrium. In terms of η_E and the orbit variables k_z, ϵ, and φ, the linearized Boltzmann equation for electrical transport is

$$\omega_c \frac{\partial \eta_E}{\partial \varphi} = \left(-\frac{\partial f_0}{\partial \epsilon}\right) v_x + W(\eta_E), \tag{3.4}$$

where $W(\eta)$ is the collision integral. For the scattering of an electron from the state $\vec{k}$ to the state $\vec{k}'$ by an impurity or a phonon, $W(\eta)$ is given by[10]

$$W(\eta) = -\frac{1}{k_B T}\frac{1}{4\pi^3}\int d\vec{k}'(\psi - \psi')P(\vec{k},\vec{k}'), \tag{3.5}$$

where

$$\eta = \left(-\frac{\partial f_0}{\partial \epsilon}\right)\psi \tag{3.6}$$

and the integration extends over the Brillouin zone. $P(\vec{k},\vec{k}')$ is related to the scattering rate $Q(\vec{k},\vec{k}')$ through $P(\vec{k},\vec{k}') = f_0(\epsilon)[1 - f_0(\epsilon')]Q(\vec{k},\vec{k}') = P(\vec{k}',\vec{k})$. For the scattering of an electron from the state $\vec{k}_1$ to the state $\vec{k}_1'$ by an electron which is scattered from the state $\vec{k}_2$ to the state $\vec{k}_2'$, $W(\eta_1)$ is given by

$$W(\eta_1) = -\frac{1}{k_B T}\left(\frac{1}{4\pi^3}\right)^3 \int d\vec{k}_1' \int d\vec{k}_2' \int d\vec{k}_2 \cdot$$

$$(\psi_1 + \psi_2 - \psi_1' - \psi_2')P(\vec{k}_1,\vec{k}_2;\vec{k}_1',\vec{k}_2'). \tag{3.7}$$

In this case $P(\vec{k}_1,\vec{k}_2;\vec{k}_1',\vec{k}_2')$ is related to the scattering rate $Q(\vec{k}_1,\vec{k}_2;\vec{k}_1',\vec{k}_2')$ through $P(\vec{k}_1,\vec{k}_2;\vec{k}_1',\vec{k}_2') = f_0(\epsilon_1)f_0(\epsilon_2)[1 - f_0(\epsilon_1')][1 - f_0(\epsilon_2')]Q(\vec{k}_1,\vec{k}_2;\vec{k}_1',\vec{k}_2') = P(\vec{k}_1',\vec{k}_2';\vec{k}_1,\vec{k}_2)$.

Following the treatment of LAK, at high fields the solution η_E of Eq. (3.4) can be written as a series of powers of 1/H:

$$\eta_E = \eta_E^{(0)} + \frac{1}{H}\eta_E^{(1)} + \frac{1}{H^2}\eta_E^{(2)} + \cdots . \tag{3.8}$$

Inserting this series in Eq. (3.4), assuming that the scattering rate Q does not depend upon H, and equating coefficients of the same power of 1/H, yields

$$\frac{\partial \eta_E^{(0)}}{\partial \varphi} = 0, \tag{3·9}$$

$$\left(\frac{\omega_c}{H}\right) \frac{\partial \eta_E^{(1)}}{\partial \varphi} = \left(-\frac{\partial f_0}{\partial \epsilon}\right) v_x + W(\eta_E^{(0)}), \tag{3·10}$$

$$\left(\frac{\omega_c}{H}\right) \frac{\partial \eta_E^{(2)}}{\partial \varphi} = W(\eta_E^{(1)}), \text{ etc.} \tag{3·11}$$

Eq. (3·9) has the solution $\eta_E^{(0)} = C_E^{(0)}(k_z, \epsilon)$. Each coefficient must be a single-valued function of φ. Thus $\eta^{(1)}$ is single-valued, provided that

$$\oint W(C_E^{(0)}) d\varphi = 0, \tag{3·12}$$

where use has been made of the fact that $\oint v_x d\varphi = 0$ for closed orbits. For either choice of the collision integral given by Eq. (3·5) or (3·7), the solution of Eq. (3·12) is $C_E^{(0)} = \left(-\frac{\partial f_0}{\partial \epsilon}\right)$. const. (see Appendix B). The constant is determined by the condition that the total number of electrons be conserved. This condition is satisfied only if the constant is zero. Thus $C_E^{(0)} = 0$.

The solution of Eq. (3·10) is

$$\eta_E^{(1)} = \frac{H}{\omega_c}\left(-\frac{\partial f_0}{\partial \epsilon}\right)\left[C_E^{(1)}(k_z, \epsilon) + \int_0^{\varphi} v_x d\varphi'\right]. \tag{3·13}$$

The function $C_E^{(1)}$ is determined within a constant by the condition that $\eta_E^{(2)}$ be single-valued, that is

$$\oint W(\eta_E^{(1)}) d\varphi = 0 . \tag{3·14}$$

In general this equation has no simple solution. Equation (3·14) and the condition that the total number of electrons be conserved determine $\eta_E^{(1)}$ uniquely. Finally, the solution of Eq. (3·11) is

$$\eta_E^{(2)} = \frac{H}{\omega_c}\left[C_E^{(2)}(k_z, \varepsilon) + \int_o^{\varphi} W(\eta_E^{(1)})d\varphi'\right]. \qquad (3\cdot15)$$

The function $C_E^{(2)}$ can be determined by following the same procedure used to determine $C_E^{(1)}$, but is not needed in this treatment.

Once η_E has been determined, the conductivity tensor element σ_{xx} can be calculated from

$$\sigma_{xx} = \frac{e^2}{4\pi^3} \int d\vec{k}\, v_x\, \eta_E\ , \qquad (3\cdot16)$$

where the integration extends over the Brillouin zone. If several bands are present, the results for each band should be summed. Using Eq. (3·8) for η_E, Eq. (3·16) for σ_{xx}, and the fact that $d\vec{k} = (-eH/\hbar^2 c\omega_c)\, dk_z\, d\varepsilon d\varphi$, one obtains a series expression for σ_{xx} in powers of $1/H$. The term proportional to $1/H$ vanishes by virtue of the fact that $\oint v_x d\varphi \int_o^{\varphi} v_x d\varphi' = 0$. The term proportional to $1/H^2$ does not vanish and is given by

$$\sigma_{xx} \sim -\frac{e^3}{4\pi^3\hbar^2 c} \int \frac{dk_z}{\omega_c} \int d\varepsilon \oint d\varphi v_x \frac{1}{\omega_c}\int_o^{\varphi} W(\eta_E^{(1)})d\varphi'\ . \qquad (3\cdot17)$$

The integral over φ can be simplified by integrating by parts:

$$\oint d\varphi v_x \frac{1}{\omega_c}\int_o^{\varphi} W(\eta_E^{(1)})d\varphi' =$$

$$\left[\oint W(\eta_E^{(1)})d\varphi'\right]\left[\frac{1}{\omega_c}\left(C_E^{(1)} + \oint v_x d\varphi\right)\right]$$

$$- \oint d\varphi' W(\eta_E^{(1)})\, \frac{1}{\omega_c}\left(C_E^{(1)} + \int_o^{\varphi'} v_x d\varphi\right). \qquad (3\cdot18)$$

The first term on the right-hand side of Eq. (3·18) vanishes by virtue of Eq. (3·14). Direct substitution of Eq. (3·18) into (3·17) and a change of variables back to Cartesian coordinates yields the simple result:

$$a_{xx} = \frac{e^2}{4\pi^3} \int d\vec{k}\left[-W(\eta_E^{(1)})\psi_E^{(1)}\right], \qquad (3\cdot19)$$

where a_{xx} is the coefficient on the $1/H^2$ term in σ_{xx}, and $\psi_E^{(1)}$ is related to $\eta_E^{(1)}$ by Eq. (3·6).

A similar expression for A_{xx}/T can be derived in the same manner. With a temperature gradient $(-\nabla_x T)$ and zero electric field, the linearized Boltzmann equation is

$$\omega_c \frac{\partial \eta_T}{\partial \varphi} = \left(-\frac{\partial f_0}{\partial \epsilon}\right) u v_x + W(\eta_T), \tag{3·20}$$

where $u = (\epsilon-\mu)/k_B T$ and $(-k_B \nabla_x T)\eta_T = f - f_0$. Using the defining relation

$$(\varkappa_e)_{xx} = \frac{k_B^2 T}{4\pi^3} \int d\vec{k}\; u v_x \eta_T, \tag{3·21}$$

one obtains

$$\frac{A_{xx}}{T} = \frac{k_B^2}{4\pi^3} \int d\vec{k} \left[-W(\eta_T^{(1)})\psi_T^{(1)}\right], \tag{3·22}$$

where A_{xx} is the coefficient of the $1/H^2$ term in $(\varkappa_e)_{xx}$, and $\psi_T^{(1)}$ is related to $\eta_T^{(1)}$ by Eq. (3·6). The quantity $\eta_T^{(1)}$ is given by

$$\eta_T^{(1)} = \frac{H}{\omega_c}\left(-\frac{\partial f_0}{\partial \epsilon}\right) u \left[C_T^{(1)}(k_z, \epsilon) + \int_0^{\varphi} v_x \, d\varphi'\right], \tag{3·23}$$

and the function $C_T^{(1)}$ is determined by the condition:

$$\oint W(\eta_T^{(1)}) d\varphi = 0 \; . \tag{3·24}$$

To calculate a_{xx} and A_{xx}/T from Eqs. (3·19) and (3·22) for a specific scattering mechanism, it is first necessary to determine $\eta_E^{(1)}$ and $\eta_T^{(1)}$. In general, both quantities will depend upon the scattering mechanism through $C_E^{(1)}$ and $C_T^{(1)}$. However, if the magnetic field is oriented along a twofold or higher-symmetry axis, and each orbit possesses this same symmetry with respect to the rest of the zone, $\eta_E^{(1)}$ and $\eta_T^{(1)}$ are determined uniquely by symmetry and do not

depend upon the scattering mechanism, as shown below.

In the remainder of this section, it is assumed that $\vec{H}$ is directed along a twofold symmetry axis. This will naturally also include the case in which $\vec{H}$ is directed along a fourfold symmetry axis, corresponding to the experimental situation considered in this paper. The E and T subscripts on η can be dropped temporarily, for the arguments given here are identical for electrical and thermal transport. With each orbit possessing twofold symmetry about $\vec{H}$, it follows that $v_x(\varphi+\pi) = -v_x(\varphi)$, and it can be shown (Appendix C) that the solution to the Boltzmann equation must also have the same property; in particular, $\eta^{(1)}(\varphi + \pi) = -\eta^{(1)}(\varphi)$, or equivalently,

$$\oint \eta^{(1)}(\varphi)d\varphi = 0 \ . \tag{3·25}$$

This condition determines $\eta^{(1)}$ uniquely. Since $W[\eta^{(1)}(\varphi + \pi)] = -W[\eta^{(1)}(\varphi)]$, Eqs. (3·14) or((3·24) will be automatically satisfied by choice of $\eta^{(1)}$ that satisfies Eq. (3·25).[11] Using Eqs. (3·13) and (3·23) for $\eta_E^{(1)}$ and $\eta_T^{(1)}$, and the fact that $v_x d\varphi = (-\hbar c\omega_c/eH)dk_y$, one can readily show that

$$\eta_T^{(1)} = u\eta_E^{(1)} = \left(-\frac{\partial f_0}{\partial \epsilon}\right)\left(\frac{\hbar c}{e}\right)\left(-u\tilde{k}_y\right), \tag{3·26}$$

where $\tilde{k}_y$ is the y component of wave vector measured from the center of symmetry of the orbit.

If several scattering processes are present simultaneously, the collision integral $W(\eta)$ in the Boltzmann equation should be replaced by the sum of the collision integrals for each scattering mechanism. Since $\eta_E^{(1)}$ and $\eta_T^{(1)}$, given by Eq. (3·26) do not depend upon the scattering mechanism, it is clear that the high-field conductivities, given by Eqs. (3·19) and (3·22), will be the sum of the conductivities for each scattering mechanism, as if each acted separately.

Having established the additivity of the high-field conductivities for different scattering mechanisms, it is possible to consider the contribution of each mechanism separately. Using Eqs. (3·19) and (3·22) for a_{xx} and A_{xx}/T, Eq. (3·26) for $\eta_E^{(1)}$ and $\eta_T^{(1)}$, and Eq. (3·5) for $W(\eta)$, one obtains

$$a_{xx} = \left(\frac{\hbar c}{4\pi^3}\right)^2 \frac{1}{2k_B\bar{T}} \int d\vec{k} \int d\vec{k}' \left[\tilde{k}_y - \tilde{k}_y'\right]^2 P(\vec{k},\vec{k}') \tag{3·27}$$

and

$$\frac{A_{xx}}{T} = \left(\frac{k_B}{e}\right)^2 \left(\frac{\hbar c}{4\pi^3}\right)^2 \frac{1}{2k_B\bar{T}} \int d\vec{k} \int d\vec{k}' \left[u\tilde{k}_y - u'\tilde{k}_y'\right]^2 P(\vec{k},\vec{k}'). \tag{3·28}$$

If Eq. (3·7) is used for the collision integral $W(\eta)$, one obtains

$$a_{xx} = \frac{(\hbar c)^2}{(4\pi^3)^4} \frac{1}{4k_B\bar{T}} \int d\vec{k}_1 \int d\vec{k}_2 \int d\vec{k}_1' \int d\vec{k}_2'$$

$$\left[\tilde{k}_{1y} + \tilde{k}_{2y} - \tilde{k}_{1y'} - \tilde{k}_{2y'}\right]^2 P(\vec{k}_1,\vec{k}_2;\vec{k}_1',\vec{k}_2') \tag{3·29}$$

and

$$\frac{A_{xx}}{T} = \left(\frac{k_B}{e}\right)^2 \frac{(\hbar c)^2}{(4\pi^3)^4} \frac{1}{4k_B\bar{T}} \int d\vec{k}_1 \int d\vec{k}_2 \int d\vec{k}_1' \int d\vec{k}_2'$$

$$\cdot \left[u_1\tilde{k}_{1y} + u_2\tilde{k}_{2y} - u_1'\tilde{k}_{1y'} - u_2'\tilde{k}_{2y'}\right]^2 P(\vec{k}_1,\vec{k}_2;\vec{k}_1',\vec{k}_2'). \tag{3·30}$$

To this point, only intraband scattering has been considered. To illustrate the considerations involved when interband scattering is present, consider two bands, denoted by α and β, each containing a single closed sheet of the Fermi surface and possessing twofold symmetry about $\vec{H}$. The Boltzmann equations for electrical transport are given by,

$$\omega_{c\alpha} \frac{\partial \eta_{E\alpha}}{\partial \varphi_\alpha} = \left(-\frac{\partial f_0}{\partial \varepsilon_\alpha}\right) v_{x\alpha} + W_\alpha(\eta_{E\alpha};\eta_{E\beta}), \tag{3·31}$$

$$\omega_{c\beta}\frac{\partial\eta_{E\beta}}{\partial\varphi_\beta} = \left(-\frac{\partial f_0}{\partial\epsilon_\beta}\right)v_{x\beta} + W_\beta(\eta_{E\beta};\eta_{E\alpha}). \tag{3·32}$$

For the scattering of an electron by an impurity or phonon, $W_\alpha(\eta_\alpha;\eta_\beta)$ is given by

$$W_\alpha(\eta_\alpha;\eta_\beta) = -\frac{1}{k_BT}\frac{1}{4\pi^3}\Big[\int_\alpha d\vec{k}'(\psi_\alpha - \psi_{\alpha'})P_{\alpha\alpha}(\vec{k},\vec{k}') + \int_\beta d\vec{k}'(\psi_\alpha - \psi_{\beta'})P_{\alpha\beta}(\vec{k},\vec{k}')\Big]. \tag{3·33}$$

The first term represents intraband scattering of the type $\vec{k}_\alpha \to \vec{k}_{\alpha'}$, and the second term represents interband scattering of the type $\vec{k}_\alpha \to \vec{k}_{\beta'}$. The expression for $W_\beta(\eta_\beta;\eta_\alpha)$ can be obtained by permuting α and β in Eq. (3·33). An expression analogous to Eq. (3·33) can be obtained for electron-electron scattering.

The results derived earlier in this section for intraband scattering hold also for combined intra- and interband scattering. In particular, it is shown in Appendix B that $C_\alpha^{(0)} = C_\beta^{(0)} = 0$. Also $\eta_{E\alpha}^{(1)}$ and $\eta_{E\beta}^{(1)}$ are determined by Eq. (3·25) as before, and therefore are given by Eq. (3·26). Using Eq. (3·19) to calculate the contribution to a_{xx} from each band, one obtains

$$a_{xx} = \frac{e^2}{4\pi^3}\Big[\int_\alpha d\vec{k}\left\{-W_\alpha(\eta_{E\alpha}^{(1)};\eta_{E\beta}^{(1)})\psi_{E\alpha}^{(1)}\right\} + \int_\beta d\vec{k}\left\{-W_\beta(\eta_{E\beta}^{(1)};\eta_{E\alpha}^{(1)})\psi_{E\beta}^{(1)}\right\}\Big]. \tag{3·34}$$

In the case of the scattering of an electron by an impurity or phonon, Eq. (3·34) becomes

$$a_{xx} = \left(\frac{\hbar c}{4\pi^3}\right)^2\frac{1}{2k_BT}\Big[\int_\alpha d\vec{k}\int_\alpha d\vec{k}'[\hat{k}_y-\hat{k}_y']^2P_{\alpha\alpha}(\vec{k},\vec{k}') + \int_\beta d\vec{k}\int_\beta d\vec{k}'[\hat{k}_y - \hat{k}_y']^2P_{\beta\beta}(\vec{k},\vec{k}') + 2\int_\alpha d\vec{k}\int_\beta d\vec{k}'[\hat{k}_y-\hat{k}_y']^2P_{\alpha\beta}(\vec{k},\vec{k}')\Big], \tag{3·35}$$

where use has been made of the symmetry properties of the P's: $P_{\alpha\alpha}(\vec{k},\vec{k}') = P_{\alpha\alpha}(\vec{k}',\vec{k})$, $P_{\beta\beta}(\vec{k},\vec{k}') = P_{\beta\beta}(\vec{k}',\vec{k})$, and $P_{\alpha\beta}(\vec{k},\vec{k}') = P_{\beta\alpha}(\vec{k}',\vec{k})$. An analogous expression for A_{xx}/T can be derived in the same manner. The argument can also be extended to include interband electron-electron scattering, although the expressions obtained are considerably more cumbersome.

3. High-Field Conductivities: Relationship to Zero-Field Resistivities and their Temperature Dependence

In the first part of this section, I explore the relationship between the high-field conductivity formulae derived in Sec. B2 and the zero-field resistivities given by the Kohler variational principle. I consider initially a system whose Fermi surface is a single closed sheet, belonging to a single band. According to the Kohler variational principle,[12] the zero-field resistivity ρ can be written

$$\rho \leq \rho_v\{\Phi\} \equiv \frac{1}{J_x^2}\frac{1}{4\pi^3}\int d\vec{k}\left[-W\left\{\left(-\frac{\partial f_0}{\partial \epsilon}\right)\Phi\right\}\Phi\right] \qquad (3\cdot36)$$

with $J_x = 1/4\pi^3 \int d\vec{k} e v_x(-\partial f_0/\partial\epsilon)\Phi$. The trial function Φ is chosen to minimize the right-hand side of Eq. (3·36), reducing the equation to an equality. In this case $\left(-\frac{\partial f_0}{\partial \epsilon}\right)\Phi$ represents (within a constant factor) the deviation of the distribution function f from its equilibrium value f_0. The quantity J_x represents the x component of the electrical current density associated with the distribution function $f_0 + (-\partial f_0/\partial\epsilon)\Phi$. (The electric field is taken to be along the x axis.) Generally the proper choice of Φ will depend upon the scattering mechanism, and the additivity of the resistivities for different scattering mechanisms (Matthiessen's rule) will be only approximate.

I assume that the system has cubic symmetry and that the z axis is directed along a fourfold symmetry axis. A possible choice for Φ is $\hbar c\tilde{k}_x$, where $\tilde{k}_x$ is measured from the center of symmetry of the sheet.

In almost every case,[13] this will not be the best choice for Φ, and Eq. (3·36) will be an inequality. However, with this choice of Φ, the denominator of Eq. (3·36) can be written

$$J_x^2 = \left(\frac{1}{4\pi^3}\int \frac{dS}{\hbar v} e v_x(\hbar c k_x)\right)^2 = \left(\frac{ec}{4\pi^3}\cdot\frac{1}{3}\int dS\ \hat{n}\cdot\vec{K}\right)^2, \qquad (3\cdot37)$$

where dS is an element of the Fermi surface, and $\hat{n}$ is a unit vector normal to the surface, directed outward from the surface if the sheet is an electron surface, and inward if the sheet is a hole surface. The integral $\frac{1}{3}\int dS\ \hat{n}\cdot\vec{K}$ is just the volume enclosed by the Fermi surface, which is $4\pi^3$ times the number of states n enclosed. Consequently, the denomincator has the value $(nec)^2$. Since the z axis is assumed to be a fourfold symmetry axis, the trial function $\Phi = \hbar c\tilde{k}_x$ appearing in the numerator of Eq. (3·36) can be replaced by $-\hbar c\tilde{k}_y$ without changing the value of the numerator. Then it follows from Eqs. (3·19) and (3·26), that the numerator is identically equal to a_{xx}. Consequently, $\rho \leq \rho_v\{\hbar c k_x\} \equiv a_{xx}/(nec)^2$. However, $a_{xx}/(nec)^2$ is just the high-field magnetoresistivity ρ_{xx} of the material, so that $\rho \leq \rho_v\{\hbar c k_x\} \sim \rho_{xx}$.

This treatment can be easily generalized to systems in which portions of the Fermi surface are distributed among several bands. For example, if there are two bands α and β, the numerator of Eq. (3·36) is identical to Eq. (3·34), if $e\psi_{E\alpha}^{(1)}$ and $e\psi_{E\beta}^{(1)}$ appearing in Eq. (3·34) are replaced by the trial functions Φ_α and Φ_β, respectively. The quantity J_x in Eq. (3·36) represents the total x component of the current density, corresponding to the distribution function $f_0 + \left(-\frac{\partial f_0}{\partial \epsilon_\alpha}\right)\Phi_\alpha$ for the α band and $f_0 + \left(-\frac{\partial f_0}{\partial \epsilon_\beta}\right)\Phi_\beta$ for the β band. Following the earlier arguments, one obtains

$$\rho \leq \frac{a_{xx}}{[(n_e - n_h)ec]^2} \sim \rho_{xx}, \qquad (3\cdot38)$$

and for the thermal case,

$$WT \leq \frac{A_{xx}/T}{[L_0(n_e - n_h)ec]^2} \sim W_{xx}T \qquad (3\cdot39)$$

where n_e and n_h are the numbers of electrons and holes respectively.

While these results by themselves may not be very surprising, the derivation is interesting because it indicates that in an uncompensated ($n_e \neq n_h$) metal, the difference between the high-field magnetoresistivity and the zero-field resistivity is a measure of the error produced when the trial function $\Phi = \hbar c\tilde{k}_x$ ($\Phi = \hbar cu\tilde{k}_x$ in the thermal case) for each sheet is used to calculate the zero-field resistivity by the Kohler variational principle. If the system is compensated ($n_e = n_h$), the right-hand sides of Eqs. (3·38) and (3·39) diverge. This reflects the fact that the trial function $\hbar c\tilde{k}_x$ for each sheet yields a vanishing total current, while the correct trial function for each sheet would give a finite total current.

In view of the similarity of the variational expression for ρ and the expression for a_{xx} [for example, compare Eqs. (3·36) and (3·19)], it <u>may</u> be reasonable to expect that ρ and a_{xx} (or WT and A_{xx}/T in the thermal case) would have similar temperature dependences. This is especially evident for the simple case in which a relaxation time τ exists. In this case $W(\eta) = -\eta/\tau$ and both ρ and a_{xx}, as well as WT and A_{xx}/T, depend upon τ in the same way: Each is proportional to $1/\tau$. In the remainder of this section I consider the temperature dependences of a_{xx} and A_{xx}/T expected for impurity, electron-electron, and electron-phonon scattering.

Of these scattering mechanisms, impurity scattering is the simplest to discuss. Such scattering is elastic and leads to values of a_{xx} and A_{xx}/T that are temperature independent and related by the Wiedemann-Franz law: i.e., $A_{xx}/Ta_{xx} = L_0$.

The temperature dependence of a_{xx} and A_{xx}/T for electron-electron scattering is determined mainly by the Fermi factors contained in $P(\vec{k}_1,\vec{k}_2;\ \vec{k}_1',\vec{k}_2')$. This reflects the operation of the Pauli exclusion

principle, which confines the scattering to a region within k_BT of the Fermi energy, resulting in a characteristic T^2 temperature dependence for the high-field conductivities, a_{xx} and A_{xx}/T. This T^2 behavior should be largely independent of the Fermi surface topology,[14] and should occur for interband as well as intraband processes.

The situation for electron-phonon scattering is much less clear. In the simple metals in the absence of a magnetic field, the Bloch theory,[15] which treats only normal processes, predicts a T^5 dependence of ρ and a T^3 dependence of WT at low temperatures. Umklapp processes,[16] not treated in the Bloch theory, must be dealt with on a metal to metal basis, since the contribution of these processes to the resistivities are sensitive to the positions of the Bragg planes relative to the Fermi surface and to the form of the pseudopotential. Theoretical calculations have indicated for some time that umklapp scattering plays a dominant role in determining the electrical resistivity,[17] and there is growing evidence that umklapp processes do in fact cause serious deviations from a simple low-temperature T^5 behavior in some metals.[18]

While the role of the electron-phonon scattering is still incompletely understood in the simple metals, it is even less well understood in the transition metals. The problem is difficult for several reasons. First, the Fermi surface of a typical transition metal does not generally even resemble the surface that would be derived from a nearly-free-electron model. Secondly, the wavefunctions generally have significant s-d character and the pseudopotential cannot yet be calculated reliably, so that the matrix element for electron-phonon scattering is uncertain. Consequently, for lack of a better alternative, experimentalists have had to assume, without much theoretical justification, that the simple T^5 and T^3 behavior for ρ and WT can be used to describe electron-phonon scattering at low temperatures in transition metals. One might expect by analogy that the contribution of electron-

phonon scattering to a_{xx} and A_{xx}/T would be proportional to T^5 and T^3, respectively, but, as far as the transition metals are concerned, it is probably wise to apply these results with considerable caution.

C. Experimental Results

The tungsten sample used in the experiment was spark-cut from a longer 3-mm-diam zone-refined crystal, which had a residual resistivity ratio, $\rho(299K)/\rho(0K)$, of 63,000.[19] The rod axis was parallel to the [110] direction (taken as the x axis), and the magnetic field $\vec{H}$ was oriented normal to the rod axis along the [001] direction (z axis). Measurements of the transverse electrical and thermal magnetoresistivities ρ_{xx} and W_{xx} were made in the conventional potentiometric manner in separate experiments.

The cryostat used was identical to the one described in the previous chapter, except that the sample was mounted horizontally, rather than vertically, so that a superconducting solenoid could be used to produce a magnetic field transverse to the sample. In the thermal measurements, the temperature difference created between two points on the sample by a heat current was measured by means of two matched Allen Bradley 56Ω, 1/10 W carbon resistors soldered to copper rings which had been electroplated to the sample. For the electrical measurements, the thermometers were left in place, a current lead was attached to the free end of the sample, and potential leads were attached to the sample at the thermometers.

It is worth mentioning that at high magnetic fields the use of ring contacts rather than point contacts will not seriously perturb the current distribution in the sample, provided that the sample is compensated and the magnetic field is oriented along a high-symmetry direction. Although the rings will short-circuit the Hall electric field locally, under these circumstances the Hall field is so small compared to the electric field along the specimen axis that the effect is negligible. On the other hand, if the specimen were uncompensated,

just the reverse would be true, and the current distribution would be seriously perturbed.

The thermometers were calibrated during each experiment (in zero magnetic field) against a standard germanium resistance thermometer. Small corrections for the magnetoresistance of the carbon resistors[20] were made, but were so small for the field strengths used, that they were hardly necessary. During the thermal measurements, heat currents of 0.1 to 1 mW were used to generate temperature differences of about 200 mK at each field, allowing measurement of W_{xx} to a precision of better than 2%. All thermometer and heater leads to the sample were constantan, and the heat leak through these leads were negligible. It was verified that the heat lost through the vacuum surrounding the sample was also negligible by comparing measurements taken with the sample at different temperatures relative to its environment.

The results of the electrical measurements are summarized in Figure 3.1. In this figure, H^2/ρ_{xx} is plotted against T^2 for several values of the magnetic field. The purpose of plotting the data in this manner is first to show the field dependence of ρ_{xx}, and second, to show the temperature dependence of $H^2/\rho_{xx} \sim a_{xx}$ (Eq. (3·1)) in the high-field limit. It is clear from the figure that ρ_{xx} is nearly proportional to H^2, the exponent being approximately 1.96. Small deviations from the H^2 law were observed in earlier work by Fawcett,[21] but were not observed in a more recent study by Long.[22] It is not certain whether the deviations observed in this study are an intrinsic effect, or merely an artifact caused by the finite width of the electroplated copper rings which were used as potential contacts. In any case, the deviations pose no serious problem in the interpretation of the measurement, and will not be pursued further.

The temperature dependence of $H^2/\rho_{xx} \sim a_{xx}$ is nearly quadratic, but increases at a somewhat faster rate at higher temperatures. For this sample, the temperature dependent part of a_{xx} is roughly 30% of

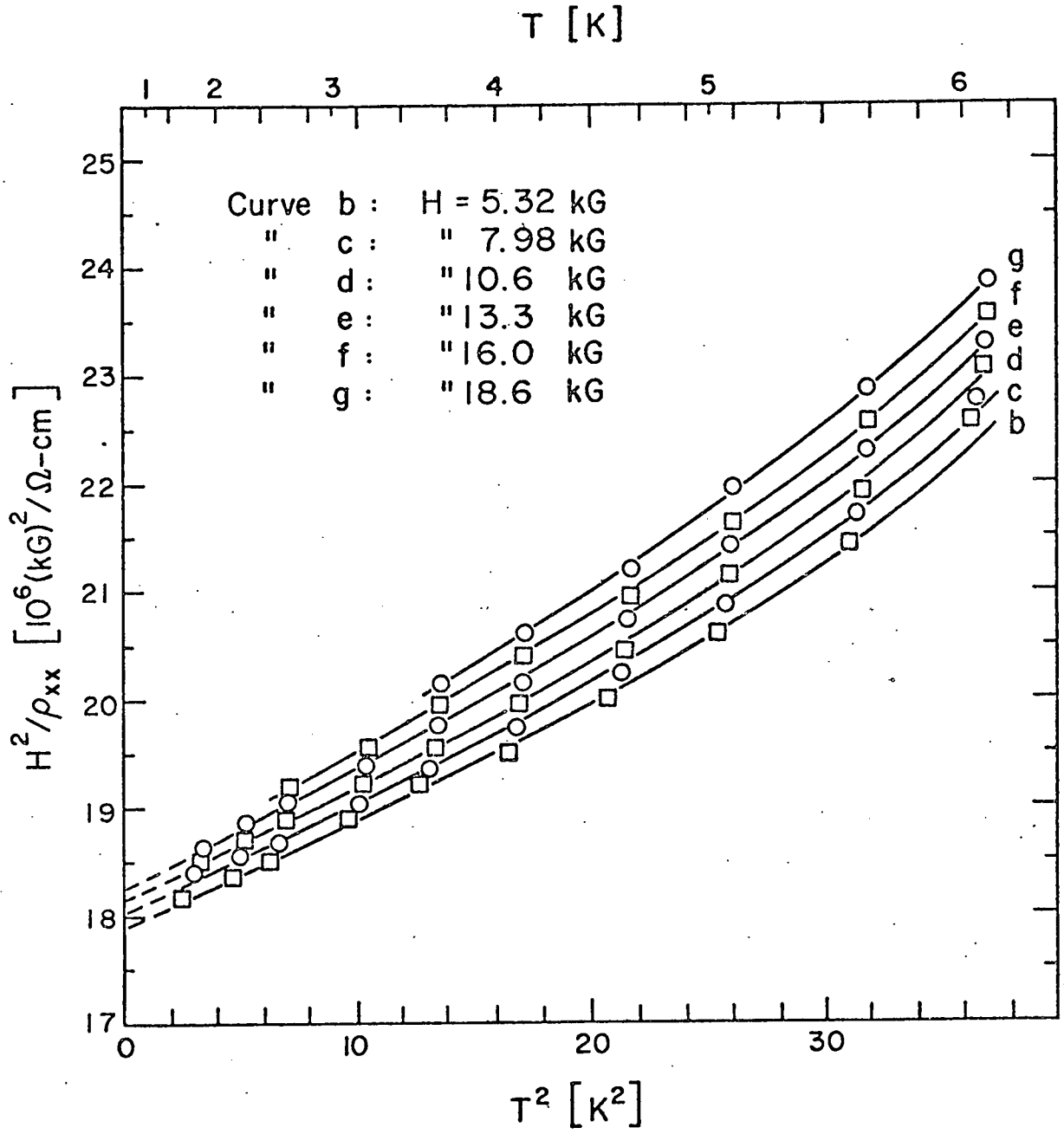

Figure 3.1. Variation of H^2/ρ_{xx} with T^2 for various values of the magnetic field H.

the residual part at 6 K. It is interesting to note that the zero-field resistivity ρ of the same sample measured in an earlier experiment showed a similar temperature dependence.[1] Furthermore, the temperature dependent part of the zero-field resistivity was also about 30% of the residual part at 6 K.

There is little doubt that the high-field regime has been reached in this sample at the magnetic fields used. At 13.3 kG and 4 K the resistance had increased by nearly five orders of magnitude over its value at zero field. Furthermore, a measurement of ρ_{xy} indicated that it was about 300 times smaller than ρ_{xx} at 13.3 kG and 4 K, so that Eq. (3·1) was valid for all field strengths used in this study.

The results of the thermal measurements are summarized in Figure 3.2, in which $H^2/W_{xx}T$ is plotted against temperature for several values of the magnetic field. To compare these results with Eq. (3·2), these data have been replotted in Figures 3.3a and 3.3b as $1/W_{xx}T$ versus $1/H^2$ for several temperatures. The agreement with Eq. (3·2) is remarkable. In particular, the intercepts give the values of κ_g/T at each temperature, and these have been plotted against temperature in Figure 3.4. As can be seen from this figure, κ_g/T has a very plausible linear temperature dependence given by $\kappa_g/T \approx 0.5\ T$ mW/cm-K^2. According to Eq. (3·2), the slope of each line in Figure 3 is the value of A_{xx}/T for that temperature. These slopes have been plotted against T^3 in Figure 3.5, demonstrating that the temperature dependent part of A_{xx}/T has an almost precisely T^3 behavior below 6 K. In contrast, the zero-field measurements of WT showed an almost precisely T^2 behavior below 6 K.[1]

In the derivation of Eq. (3·2) I neglected thermoelectric effects which arise due to the fact that the thermal magnetoresistivity W_{xx} was measured under the condition of zero electric current rather than zero electric field in the sample. The dominant correction due to these effects is a term $\rho_{xx}(\epsilon''_{xy})^2$ that should be added to the right-

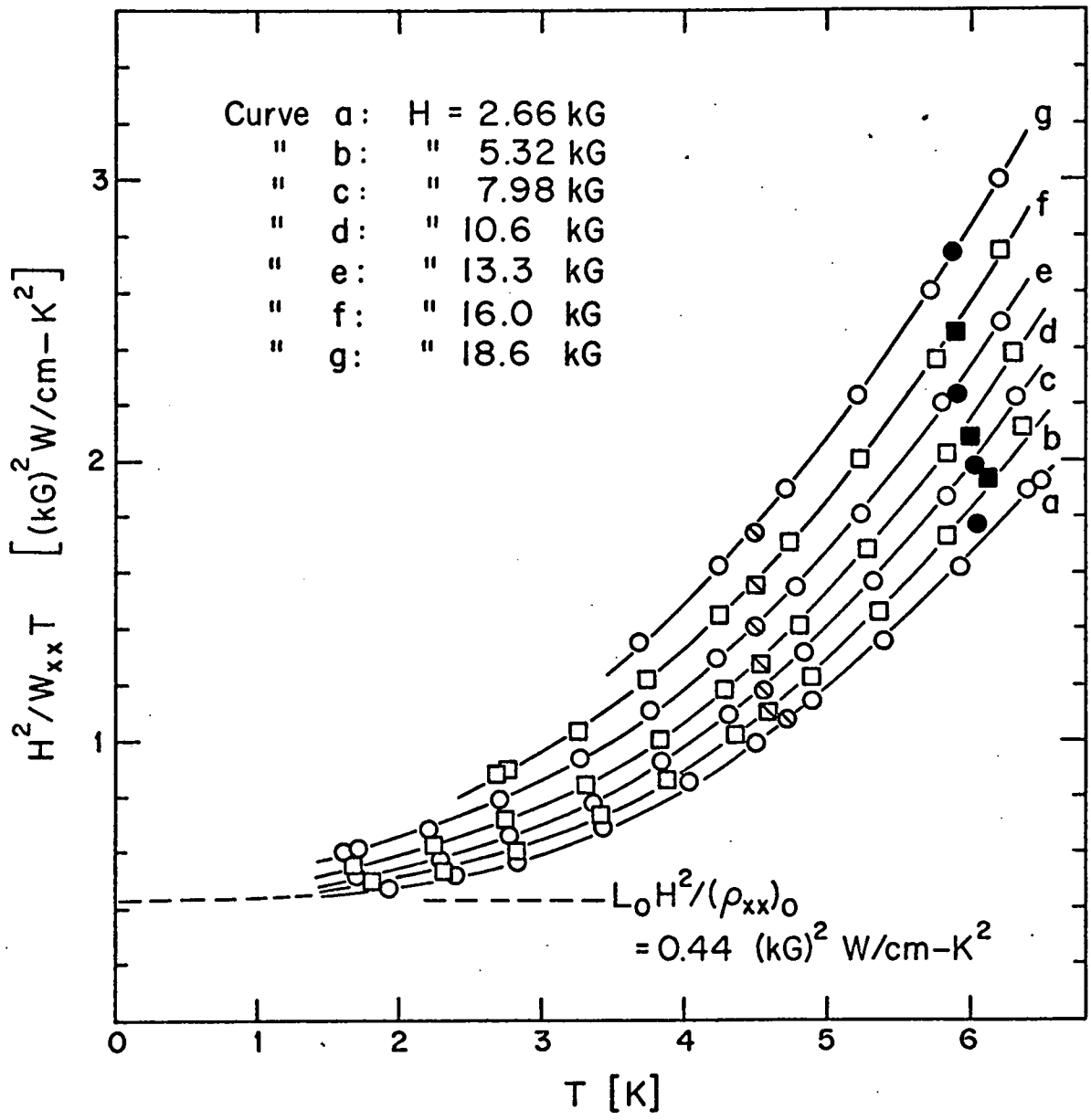

Figure 3.2 Variation of $H^2/W_{xx}T$ with temperature for various values of of the magnetic field H. The slashed data points were taken in a separate experiment with no change in the cryostat. The solid data points were taken after changing the separation of the thermometers on the sample. The dashed line indicates the residual value of $H^2/W_{xx}T$ obtained by the Wiedemann-Franz law.

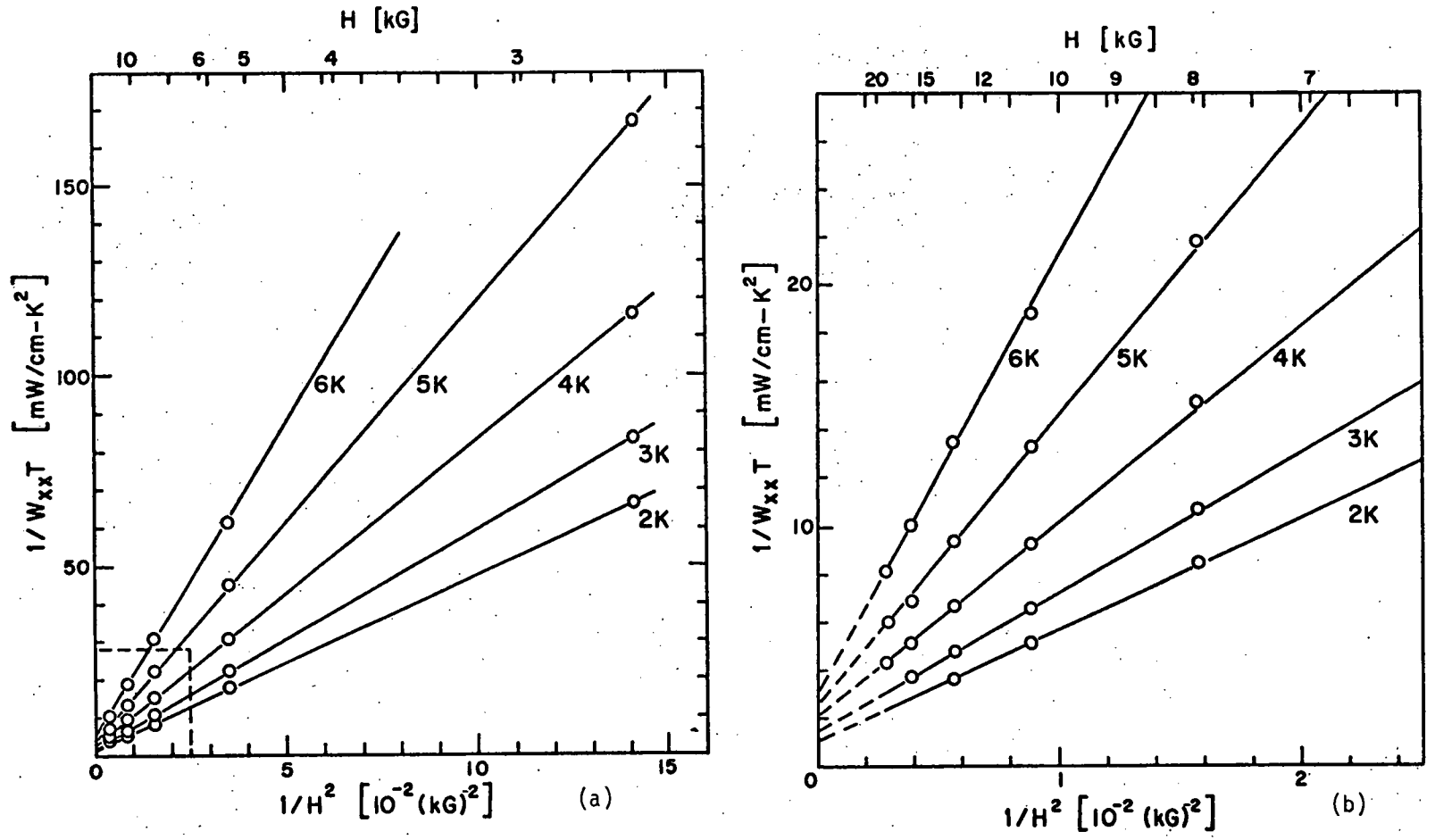

Figure 3.3. Plot of $1/W_{xx}T$ as a function of $1/H^2$ for several temperatures. In (a) some of the data within the dashed box has been omitted for clarity. The data falling within the dashed box has been plotted in (b).

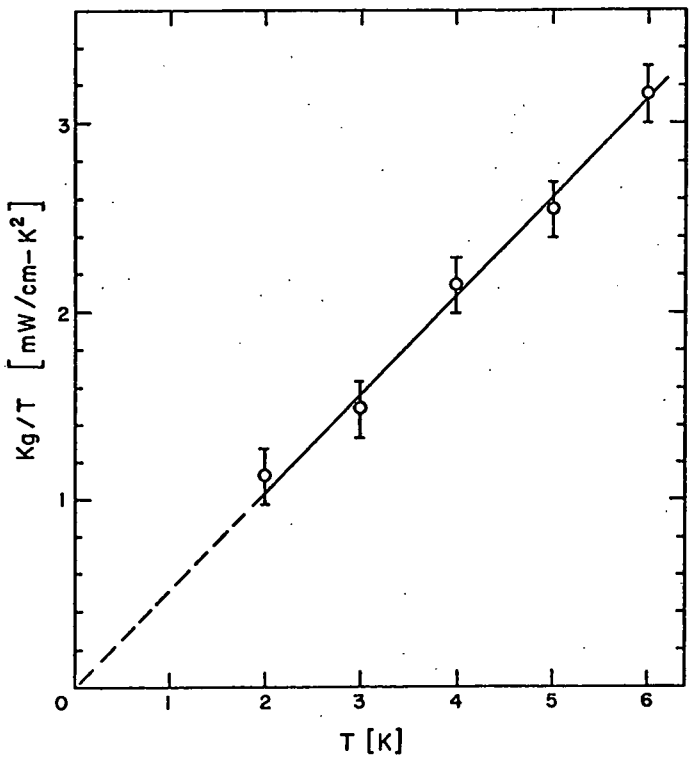

Figure 3.4. Lattice thermal conductivity divided by temperature as a function of temperature.

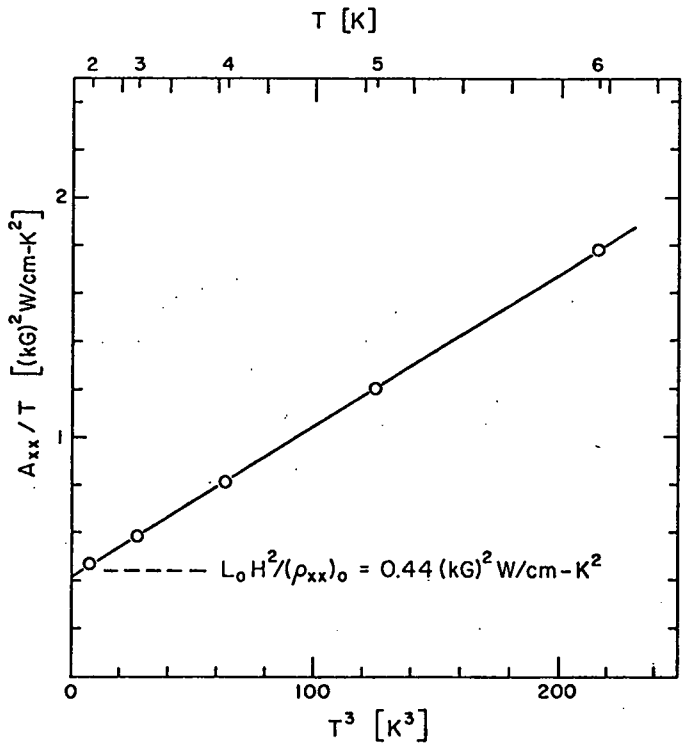

Figure 3.5 Plot of A_{xx}/T as a function of T^3. The values of A_{xx}/T were obtained from the slopes of the lines of Fig. 3.4. The precision of each value is approximately 1%.

hand side of Eq. (3·2). The quantities ρ_{xx} and ϵ''_{xy} are elements of the electrical resistivity and thermoelectric power tensors, respectively.[23] At high fields this term becomes independent of magnetic field and has the value $\rho_{xx}(c\gamma T/H)^2$, where γ is the coefficient of the electronic specific heat per cm^3 of electrons. For the tungsten sample used in this study, this term has the value 0.1 mW/cm-K^2 at 4 K.[24] Since this is at <u>least</u> 20 times smaller than $1/W_{xx}T$ for all values of the magnetic field at this temperature, the correction is of little consequence and can be ignored.

D. Discussion

One of the principal findings of this investigation is that the magnetic field dependences of both σ_{xx} and κ_{xx} follow closely the predictions of the high-field semiclassical theory, provided that thermal conduction by the lattice is taken into account. The measurements indicate that the lattice conductivity κ_g is proportional to T^2, as expected for a pure metal in which the phonons are scattered principally by the conduction electrons.[25] Furthermore, the temperature dependence, as well as the magnitude of κ_g is in good agreement with measurements made on transition metal alloys.[26] The first attempts to measure the lattice conductivity of tungsten were made over three decades ago by de Haas and de Nobel and subsequently by de Nobel, but were hampered by the lack of specimens of sufficient purity.[27] Very recently, a successful measurement of the lattice conductivity has been made by Long[28] in a tungsten crystal of higher purity than was available to de Haas and de Nobel. The measurements of κ_g reported here and reported by Long are in substantial agreement, and, as shown by Long, agree within better than a factor of 2 with reasonable theoretical estimates of κ_g.

The temperature dependences of the high-field electrical conductivity $\sigma_{xx} \sim a_{xx}/H^2$ and the electronic contribution to the thermal conductivity $(\kappa_e)_{xx}/T \sim (A_{xx}/T)/H^2$ should reflect the scattering

mechanisms present in tungsten at low temperatures. It was shown in Sec. B2 that with the magnetic field $\vec{H}$ along a twofold symmetry axis, a_{xx} and A_{xx}/T are composed of the sum of the contributions of the various scattering mechanisms present in the metal, as if each mechanism acted separately. Furthermore, the expressions for a_{xx} and A_{xx}/T obtained in Sec. B2, were apart from the choice of trial function, similar to the variational expressions for ρ and WT, respectively. For this reason it was argued that the temperature dependence of a_{xx} and ρ, as well as A_{xx}/T and WT, would probably be similar. This appears to be the case for the electrical quantities, a_{xx} and ρ, but not for their thermal counterparts, A_{xx}/T and WT. In this study, a_{xx} appears to increase nearly quadratically with temperature at low temperatures, but at a somewhat faster rate at higher temperatures approaching 6 K. In a previous study at zero magnetic field,[1] ρ was found to behave in a similar fashion. On the other hand, A_{xx}/T showed an almost precisely T^3 behavior in this study, while in the previous study WT showed an almost precisely T^2 behavior. Although the zero-field results can be plausibly explained in terms of electron-electron scattering, it seems unlikely that this scattering could cause a T^3 dependence of A_{xx}/T. It may be possible to explain both the high-field and the zero-field results in terms of electron-phonon scattering, but the current understanding of the role of these processes in the transition metals is still too poor to assess this possibility properly.

I have assumed that the effect of boundary scattering on the temperature dependence of a_{xx} and A_{xx}/T can be neglected. Indeed, the previous measurements in zero magnetic field indicated that boundary scattering did not have a significant effect on the temperature dependences of ρ and WT for this sample. Moreoever, it seems reasonable that the importance of boundary scattering should decrease as the magnetic field is increased, since the fraction of electrons striking the boundaries is reduced.

There is one assumption made in Sec. B2 that should be examined in the context of the tungsten Fermi surface. The tungsten Fermi surface has portions located in the second, third, and fourth Brillouin zones.[29] The second zone consists of an array of six small ellipsoidal hole pockets located at N (at the centers of the <110> zone faces), and the third zone consists of an octahedral-shaped hole surface located at H (the <100> zone vertex). The fourth zone contains the electron "jack" centered in the zone at Γ. In Sec. B2 it was assumed that all orbits have at least twofold symmetry about $\vec{H}$. Although $\vec{H}$ was directed along a fourfold symmetry axis in the experiment, there are a number of orbits that do not possess even twofold symmetry about this same axis. First, there are the orbits formed by the intersection of the "knobs" (but not the "necks") of the electron "jack" with a plane perpendicular to the magnetic field. These orbits occur on only a small fraction of the Fermi surface, so their contribution to the conductivities can be neglected without much error.[30] Second, four of the six hole ellopsoids taken individually do not have any special symmetry with respect to the rest of the zone. However, the surfaces are ellipsoidal, so that $v_x(\varphi + \pi) = -v_x(\varphi)$ for orbits on these surfaces. Although it does not follow that Eq. (3·25) will hold for an arbitrary scattering mechanism, Eq. (3·25) does hold in the relaxation-time approximation. Consequently, the assumption that $\eta^{(1)}$ for these surfaces is given by Eq. (3·26) should be a good starting point for calculating the contribution of these sheets to the conductivities.

I now turn to the experimental results reported by Long.[28] In that study the extraction of the lattice thermal conductivity from the measurements was based on the phenomenological expression:

$$\kappa_{xx}(H,T) = TL_1(T)\sigma_{xx}(H,T) + \kappa_g(T) \ . \qquad (3\cdot40)$$

This equation can be shown to be a simple consequence of the high-field theory. Long's crystal was oriented with the magnetic field along the [001] direction, so that all the arguments given in Sec. B apply. Equation (3·40) is equivalent to Eq. (3·2), which can be written as,

$$\varkappa_{xx}(H,T) = T\left(\frac{A_{xx}(T)}{Ta_{xx}(T)}\right)\sigma_{xx}(H,T) + \varkappa_g(T), \qquad (3\cdot41)$$

showing that $L_1(T) = A_{xx}(T)/Ta_{xx}(T)$. Thus the assumption made by Long that L_1 does not depend upon H is well justified at high fields. In Long's sample, the temperature dependent part of a_{xx} was only a small fraction of the residual part; consequently, the temperature dependence of L_1 was determined by that of A_{xx}/T. It was found in this study that A_{xx}/T varies almost precisely as T^3, while Long has fit his values of L_1 to a T^2 dependence. However, a T^3 dependence is not inconsistent with the data when the scatter is taken into account. Long's measurement of $L_2(T) = A_{xy}(T)/Ta_{xy}(T)$ can also be understood in terms of semiclassical theory. As remarked in Sec. B1, L_2 will be equal to L_o if the scattering is elastic, but will generally be greater than L_o if the scattering is inelastic. This is borne out by his measurements, which show that L_2 increases from a value near L_o at 1.5 K to a value appreciably greater than L_o at 4.2 K.

In summary, it is found that the magnetic field dependence of the high-field conductivities, σ_{xx} and $\varkappa_{xx}$, can be understood excellently in the context of the semiclassical magnetoresistance theory, provided that the thermal conductivity of the lattice $\varkappa_g$ is taken into account. A lattice thermal conductivity $\varkappa_g$ given by $\varkappa_g \approx 0.5\ T^2$ mW/cm-K is found experimentally, consistent with the view that the phonons are scattered mainly by the conduction electrons. The temperature dependence of the high-field conductivities is shown to yield information about low-temperature scattering mechanisms. However, when both zero-field and high-field measurements are considered together, it is found

that they cannot be explained plausibly in terms of electron-electron scattering, as was previously concluded from measurements of the zero-field resistivities.[1] Electron-phonon scattering may be responsible, but the current understanding of such scattering in the transition metals is still too poor to explore this possibility in greater detail.

REFERENCES

1. D. K. Wagner, J. C. Garland, and R. Bowers, Phys. B 3, 3141 (1971).
2. Evidence for electron-electron scattering has been obtained in field emission studies of tungsten at 20K; C. Lea and R. Gomer, Phys. Rev. Letters 25, 804 (1970).
3. I. M. Lifshitz, M. I. Azbel, and M. I. Kaganov, Zh. Eksperim. i Teor. Fiz. 31, 63 (1956) [Sov. Phys. JETP 4, 41 (1957)].
4. M. I. Azbel, M. I. Kaganov, and I. M. Lifshitz, Zh. Eksperim. i Teor. Fiz. 32, 1188 (1957) [Sov. Phys. JETP 5, 967 (1957)].
5. R. G. Chambers, Proc. Roy. Soc. (London) A238, 344 (1956).
6. The symbol $\sim$ is used to mean "equals asymptotically in the high-field limit".
7. By thermal conductivity tensor, it is meant the tensor that relates the heat current and temperature gradient in the absence of an electric field.
8. The thermal resistivity tensor is commonly measured in the absence of an electrical current, rather than in the absence of an electric field in the sample. There are therefore small corrections to Eq. (3·2) arising from the thermoelectric effects, which we have ignored. In Sec. C this correction is estimated and is shown to be negligible.
9. An example of the failure of this assumption is magnetic breakdown.
10. A discussion of the collision integral can be found in J. M. Ziman, Electrons and Phonons, (Oxford University Press, Oxford, 1960) Sec. 7.7.
11. I am grateful to C. Herring for pointing this out.
12. For a discussion of the Kohler variational principle for the electrical and thermal resistivities see F. J. Blatt, Physics of Electronic Conduction in Solids, (McGraw-Hill Book Company, New York, 1968), Sec. 5.5.

13. The exception is the case in which the sheet is spherical and a relaxation time exists. This situation might be expected to exist in a metal such as potassium when the scattering is dominated by impurity scattering. For the application to potassium and a comparison with experimental results, see H. Taub and D. K. Wagner (to be published).

14. For an illuminating discussion of this point, see C. Hodges, H. Smith, and J. W. Wilkins, Phys. Rev. B 4, 302 (1971).

15. See Ref. 10, Sec. 9.5.

16. In discussions of the simple metals it is fashionable to use the extended zone scheme, in which the Fermi surface appears as a sphere. In this scheme, the meaning of "umklapp" is different from that in the reduced zone scheme, which is the scheme used in this paper.

17. See for example, M. Bailyn, Phys. Rev. 120, 381 (1960); W. E. Lawrence and J. W. Wilkins (to be published).

18. See for example, A. C. Ehrlich, Phys. Rev. B 1, 4537 (1970); J. W. Ekin, Phys. Rev. Letters 26, 1550 (1971).

19. This sample was cut from sample W-6 of Ref. 1.

20. J. R. Clement and E. M. Quinell, Rev. Sci. Instr. 23, 213 (1952).

21. E. Fawcett, Phys. Rev. 128, 154 (1962).

22. J. R. Long, Phys. Rev. B 3, 1197 (1971).

23. Low-temperature measurements of ϵ''_{xy} have been carried out in tungsten by J. R. Long, Phys. Letters 25A, 677 (1967); Phys. Rev. B 3, 1197 (1971).

24. In mksA units this correction term is $\rho_{xx}(\gamma T/B)^2$, where B is the magnetic induction. At 10 kG the measured value of ρ_{xx} is about 5×10^{-6} Ω-cm and for tungsten γ is about 10^{-4} J/cm^3-K^2. Therefore, at 4 K, $\rho_{xx}(\gamma T/B)^2$ is 0.1 mW/cm-K^2.

25. P. G. Klemens, in Solid State Physics, edited by F. Seitz and D. Turnbull (Academic Press, Inc., New York, 1958), Vol. 7, p. 78-82.

26. R. Fletcher and D. Greig, Phil. Mag. 16, 303 (1967).

27. W. J. de Haas and J. de Nobel, Physica 5, 449 (1938); J. de Nobel, Physica 15, 532 (1949); J. de Nobel, Physica 23, 261 (1957); J. de Nobel, Physica 23, 349 (1957).

28. J. R. Long, Phys. Rev. B 3, 2476 (1971).

29. For a detailed discussion of the tungsten Fermi surface and a listing of references, see R. F. Girvan, A. V. Gold, and R. A. Phillips, J. Phys. Chem. Solids 29, 1485 (1968).

30. Estimates of the contributions of these portions of the Fermi surface to the electrical conductivity have been made in the relaxation-time approximation by J. R. Long, Phys. Rev. B 3, 1209 (1971).

CHAPTER IV

A DISCUSSION AND SOME APPLICATIONS OF HIGH-FIELD SEMICLASSICAL TRANSPORT THEORY

A. Introduction

In this chapter I explore in greater detail some of the results of the high-field semiclassical theory presented in Chapter III. For simplicity the discussion is limited to electrical transport. In Secs. B and C the high-field transverse and longitudinal magnetoresistances are discussed. Use is made of the Kohler variational principle to compare the high-field resistivities to the zero-field resistivities, so that the physical origin of the increase in resistance caused by a magnetic field can be seen. In Sec. D these results are applied to electron-phonon scattering in potassium. It is shown that under special circumstances, the temperature-dependent part of the high-field resistivity $(\rho_{xx})_T$ should be equal to the temperature-dependent part of the zero-field resistivity ρ_T^{impure} when impurity scattering is dominant. In addition, it is shown that deviations from Matthiessen's rule (at zero field) should be related to the enhancement of the temperature-dependent part of the resistance produced by a magnetic field.

B. The Transverse Magnetoresistance

In this section I use a somewhat different, more direct approach than the one used in the previous chapter. For simplicity I will limit the discussion primarily to systems whose Fermi surface consists of a single closed sheet. In keeping with the convention used in the previous chapters, ρ will always be used to mean the zero-field resistivity. Tensor elements, such as σ_{xx}, will always refer to the high-field values of these quantities, unless otherwise indicated. For example, $\sigma_{xx}(H)$ refers to the conductivity tensor element in a magnetic field of arbitrary strength and $\sigma_{xx}(0)$ refers to its zero-field value.

I begin by considering the entropy of the electron system not necessarily in equilibrium, but having a fixed total energy E and number of particles N. The entropy S is given by[1]

$$S = -\frac{k_B}{4\pi^3}\int d\vec{k}\left[f \ln f + (1-f)\ln(1-f)\right]. \qquad (4\cdot1)$$

In accordance with the second law of thermodynamics, the entropy is a maximum when the system is in thermodynamic equilibrium. In this situation the equilibrium distribution function f_0 is the Fermi distribution function $\left[1 + e^{(\epsilon-\mu)/k_BT}\right]^{-1}$, a fact that can be readily proved by maximizing S, subject to the constraint that E and N remain fixed. Under the influence of steady external fields, the entropy of the electron system in the steady state will generally be less than the entropy corresponding to the equilibrium state, and the steady-state distribution function f will generally be different from the equilibrium distribution function f_0.

Consider the time rate of entropy $\dot{S}$ of the electron system under the influence of an electric field $\vec{E}$ in the x direction and a magnetic field $\vec{H}$ in the z direction. In keeping with Eq. (3·6), the steady-state distribution function f can be written as

$$f - f_0 = eE_x\eta = eE_x\left(-\frac{\partial f_0}{\partial \epsilon}\right)\psi \ . \qquad (4\cdot2)$$

Differentiating Eq. (4·1) with respect to time and keeping terms of lowest order in ψ yields

$$\dot{S} = -\frac{1}{T}\frac{1}{4\pi^3}\int d\vec{k}\ \dot{f}\left[eE_x\psi - (\epsilon-\mu)\right] . \qquad (4\cdot3)$$

Since both S and f must be independent of time in the steady state, their time derivatives $\dot{S}$ and $\dot{f}$ are zero. The equation for $\dot{f}$ is just the Boltzmann equation, which for an isothermal system can be written (see Eq. (3·4))

$$\dot{f} = eE_x\left\{-\omega_c \frac{\partial \eta}{\partial \varphi} + \left(-\frac{\partial f_0}{\partial \epsilon}\right)v_x + W(\eta)\right\} = 0. \qquad (4.4)$$

Inserting this expression in Eq. (4.3), one finds that all the terms associated with the second term in Eq. (4.3) vanish leaving

$$\dot{S} = \frac{E_x^2}{T}\left\{\frac{e^2}{4\pi^3}\int d\vec{k}\ \omega_c \frac{\partial \eta}{\partial \varphi}\psi - \frac{e^2}{4\pi^3}\int d\vec{k}\ v_x\left(-\frac{\partial f_0}{\partial \epsilon}\right)\psi\right.$$

$$\left. + \frac{e^2}{4\pi^3}\int d\vec{k}\ [-W(\eta)\psi]\right\} = 0. \qquad (4.5)$$

The first term can be shown to be zero by changing the integration over wavevector to one over orbit variables and noting that $\oint \psi(\partial\psi/\partial\varphi)d\varphi = 0$.[2] Equation (4.5) becomes

$$\dot{S} = \frac{E_x^2}{T}\left\{-\frac{e^2}{4\pi^3}\int d\vec{k}\ v_x\left(-\frac{\partial f_0}{\partial \epsilon}\right)\psi\right.$$

$$\left. + \frac{e^2}{4\pi^3}\int d\vec{k}[-W(\eta)\psi]\right\} = 0. \qquad (4.6)$$

It is reasonable to associate the first term in brackets with the rate of entropy production due to the action of the electric field, and the second term in brackets with the rate of entropy production due to scattering. In the steady state, a balance is maintained between the two rates in accordance with Eq. (4.6).

The first term in brackets in Eq. (4.6) is just the negative of the conductivity tensor element $\sigma_{xx}(H)$. Consequently, Eq. (4.6) can be written

$$\sigma_{xx}(H) = \frac{e^2}{4\pi^3}\int d\vec{k}[-W(\eta)\psi]\ . \qquad (4.7)$$

This is a very important result and holds for all magnetic field strengths for which the Boltzmann equation itself is valid. To be of use, it is necessary to have additional information about ψ and η. At

zero field, one can make use of the variational principle to calculate the zero-field resistivity ρ. At high fields, the distribution function is known under special circumstances, so that the high-field value of σ_{xx} can be calculated directly from Eq. (4.7). There seems to be no straightforward method for calculating ψ or η at intermediate magnetic fields, so that we shall confine our attention to the zero-field and high-field cases.

The variational principle states that the distribution function that satisfies the zero-field Boltzmann equation is the one that maximizes the time rate of entropy due to scattering, subject to the constraint that the total time rate of entropy be zero in accordance with Eq. (4.6). Equation (4.6) can be satisfied by a wide class of functions. In particular, it is satisfied by the solution ψ to the Boltzmann equation for arbitrary magnetic field, and by other functions Φ, which may have no physical significance. For these functions, Eq. (4.6) serves to determine their magnitude. Using the variational principle in conjunction with Eqs. (4.6) and (4.7) and assuming that the system is cubic (in which case the zero-field conductivity tensor reduces to a scalar, and $\rho = 1/\sigma_{xx}(0)$), one can write

$$\rho \leq \rho_v\{\Phi\} \equiv \frac{\frac{1}{4\pi^3}\int d\vec{k}\left[-W\left\{\left(-\frac{\partial f_0}{\partial \epsilon}\right)\Phi\right\}\Phi\right]}{\left(\frac{1}{4\pi^3}\int d\vec{k}\, ev_x\left(-\frac{\partial f_0}{\partial \epsilon}\right)\Phi\right)^2} . \qquad (4.8)$$

This is the well known variational expression for the zero-field resistivity ρ.[3] Of course, if one chooses the actual zero-field solution $\psi_{H=0}$ to the Boltzmann equation for the trial function Φ, then Eq. (4.8) reduces to an equality with $\rho = \rho_v\{\psi_{H=0}\}$. On the other hand, if one chooses the actual solution ψ to the Boltzmann equation in an arbitrary magnetic field for the trial function Φ, then one obtains the result that $\rho \leq \rho_v\{\psi\} = 1/\sigma_{xx}(H)$. This is simply a statement of the fact that the time rate of entropy due to scattering is less in a magnetic field than in its absence.

While the zero-field distribution function is generally sensitive to the scattering mechanism, just the opposite is true of the high-field distribution function. In fact, if all orbits are closed and the magnetic field is directed along a twofold, threefold, or fourfold symmetry axis, the high-field distribution function is independent of the scattering mechanism and depends only upon Fermi surface geometry. Thus, according to Eq. (3·26) at high fields,[4]

$$\psi_{H\to\infty} \sim \left(\frac{\hbar c}{eH}\right)(-\tilde{k}_y) \ . \tag{4·9}$$

The high-field conductivity tensor element σ_{xx} can be calculated by substituting Eq. (4·9) into Eq. (4·7), and is just a_{xx}/H^2 in agreement with the discussion in Sec. IIIB.

An interesting relationship between the zero-field and high-field resistivities, ρ and ρ_{xx}, can be derived by evaluating $\rho_v\{\tilde{k}_x\}$. With the aid of Sec. IIIB3, it is not difficult to show that for a system with a single band

$$\rho \leq \rho_v\{\tilde{k}_x\} = a_{yy}/(nec)^2 \ , \tag{4·10}$$

provided the magnetic field is directed along a twofold or higher-symmetry axis, so that Eq. (4·9) applies. The quantity a_{yy}/H^2 is equal to the high-field conductivity tensor element σ_{yy}, and the expression for a_{yy} can be obtained from the expressions for a_{xx} by replacing $-\tilde{k}_y$ with $\tilde{k}_x$. In a strong magnetic field directed along a twofold or higher-symmetry axis, ρ_{xx} is just $a_{yy}/(nec)^2$, so that Eq. (4·10) becomes

$$\rho \leq \rho_v\{k_x\} \sim \rho_{xx} \ . \tag{4·11}$$

It should be emphasized that this result holds for any scattering mechanism, umklapp processes included. It is apparent from Eq. (4·11) that within the framework of the semiclassical theory the resistivity

increases or remains constant in a magnetic field, and that the amount of enhancement is related to the difference between $\tilde{k}_x$ and the actual zero-field solution $\psi_{H=0}$ to the Boltzmann equation. No enhancement will occur only if $\psi_{H=0}$ is proportional to $\tilde{k}_x$, for then $\rho = \rho_v\{\psi_{H=0}\} = \rho_v\{\tilde{k}_x\}$. The only situation for which this will occur is for a system with a spherical Fermi surface and scattering describable by a relaxation time. This observation forms the basis for the discussion in Sec. D of this chapter.

Throughout this whole discussion, the precise definition of the high-field regime has been nebulous. The onset of the high-field regime depends upon the nature of the scattering mechanism, and it is only in the case of the simplest relaxation mechanisms that a compact criterion can be set down. For example, if a relaxation time τ exists, the high-field regime is achieved when $\omega_c\tau > 1$ for all orbits. Of course, the operational definition we have adopted in the previous discussions is that the high-field regime is achieved when σ_{xx}, σ_{yy}, and σ_{xy} have approached to sufficient accuracy their asymptotic values, a_{xx}/H^2, a_{yy}/H^2, and nec/H, respectively. This can be expected to occur when the terms proportional to $1/H^4$ in σ_{xx} and σ_{yy} and the term proportional to $1/H^2$ in σ_{xy} can be neglected. Expressions for these higher-order terms can be calculated by the method of Sec. IIIB2 but are so unwieldy that they seem to be of little practical value.

In Figure 4.1 the distribution functions are illustrated for a spherical and a cubical Fermi surface in zero magnetic field and in a strong magnetic field. Since the zero-field distribution function depends strongly upon the scattering mechanism, this must be specified. If one assumes a relaxation time τ, then $\psi_{H=0} = \tau v_x$. In Figure 4.2 the situation for two bands is illustrated; the first band contains a spherical electron surface and the second a spherical hole surface. Note that at zero-field, the distribution functions are "shifted" in <u>opposite</u> directions in $\vec{k}$-space along the electric field, while at high

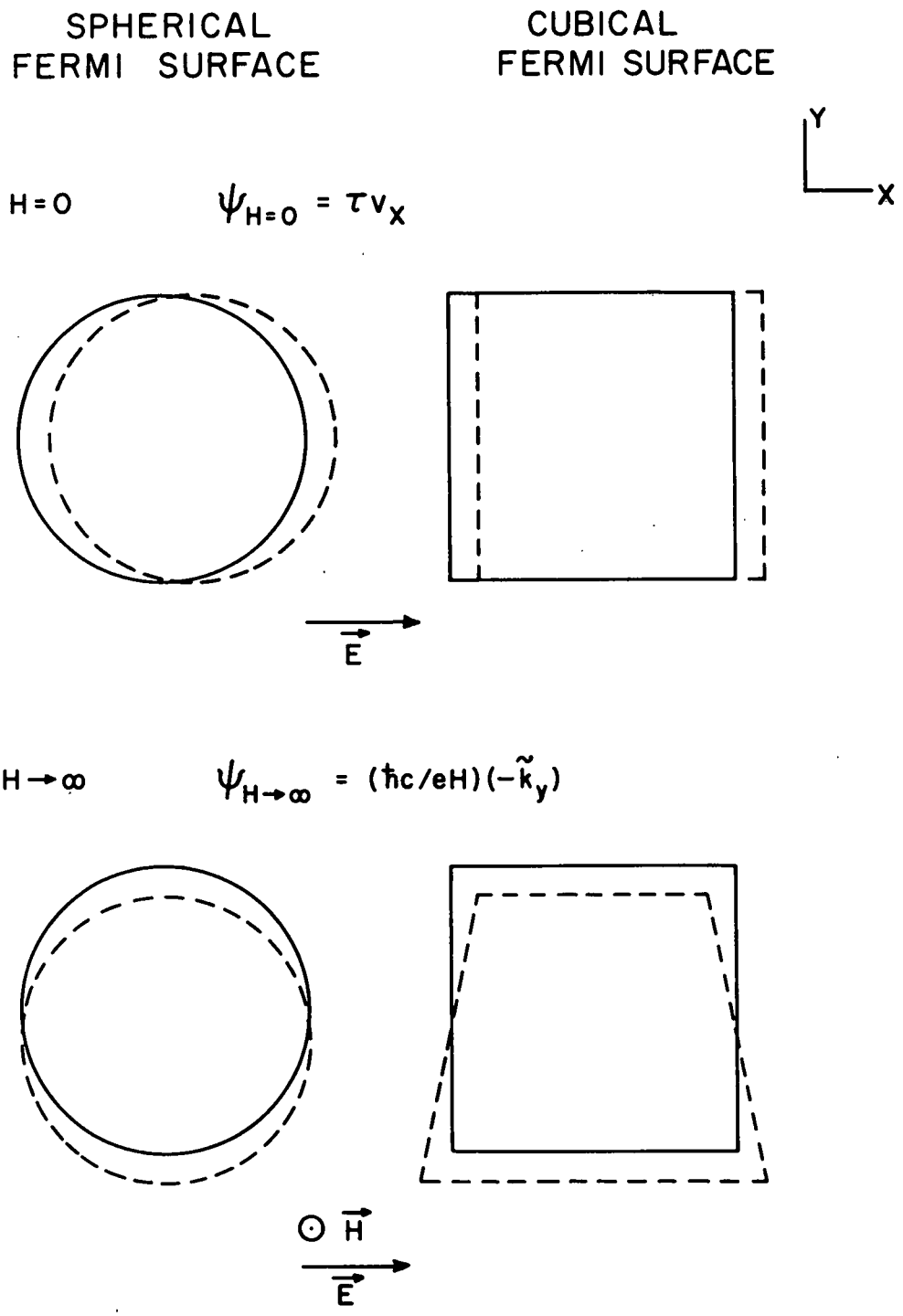

Figure 4.1. Distribution functions for spherical and cubical Fermi surfaces in zero magnetic field and in a strong magnetic field. The solid line represents the Fermi surface. The dotted line represents the change in the distribution function caused by the field, The change in the distribution function is positive if the dotted line is outside the Fermi surface and negative if it is inside.

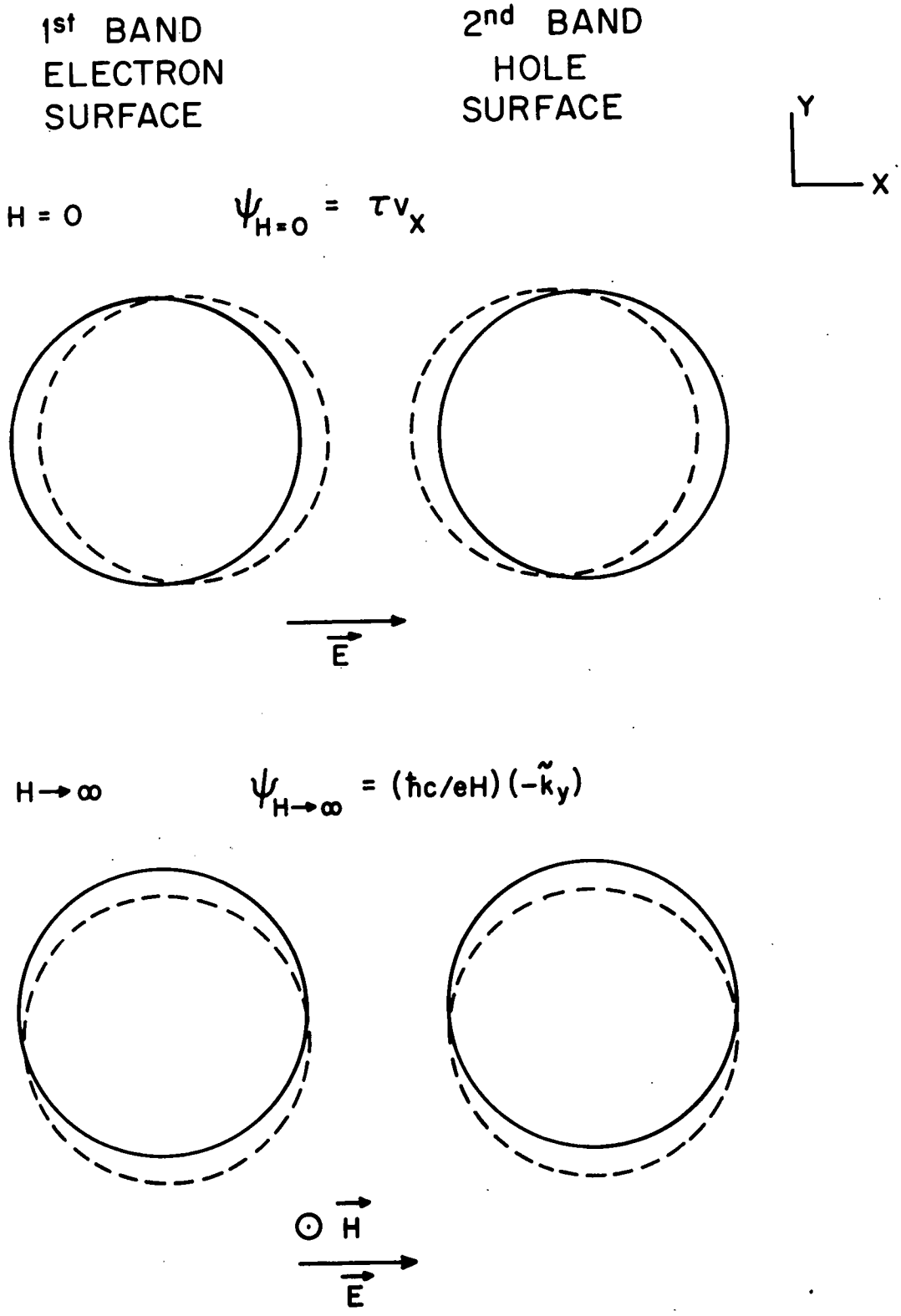

Figure 4.2. Distribution functions for a system with two bands. The interpretation of the diagrams is explained in Fig. 4.1.

fields the distribution functions are "shifted" in the same direction in $\vec{k}$-space perpendicular to the electric and magnetic fields.[5]

C. The Longitudinal Magnetoresistance

The discussion in this section is limited to systems whose Fermi surface consists of a single closed sheet. With the magnetic and electric fields along the z axis, the Boltzmann equation for electrical transport is

$$\omega_c \frac{\partial \eta}{\partial \varphi} = \left(-\frac{\partial f_0}{\partial \epsilon}\right) v_z + W(\eta) \ . \qquad (4.12)$$

By following the analysis of the previous section and calculating the time rate of entropy $\dot{S}$, one can show that

$$\sigma_{zz}(H) = \frac{e^2}{4\pi^3} \int d\vec{k}[-W(\eta)\psi] \ ; \qquad (4.13)$$

which is the analogue of Eq. (4.7).

Equation (4.13) is of little value unless more information is known about ψ and η. At zero field, we make use of the variational principle to calculate the zero-field resistivity ρ and at high fields we solve the Boltzmann equation to lowest order in 1/H. However, in contrast to the high-field distribution function for a transverse magnetic field, the high-field distribution function for a longitudinal magnetic field depends strongly upon the scattering mechanism. Thus, it is not possible to derive an explicit expression for ψ in a longitudinal magnetic field, but it is possible to obtain an implicit expression for this quantity. With this expression it is possible to relate the high-field longitudinal magnetoresistivity ρ_{zz} to the zero-field resistivity ρ by means of the Kohler variational principle, and to ascertain under what conditions an enhancement of the resistivity in a longitudinal magnetic field can be expected to occur.

In the manner of Sec. IIIB2, the solution to Eq. (4.12) can be written as a power series in 1/H. Following that treatment,

$$\frac{\partial \eta^{(0)}}{\partial \varphi} = 0 \tag{4.14}$$

$$\left(\frac{\omega_c}{H}\right) \frac{\partial \eta^{(1)}}{\partial \varphi} = \left(-\frac{\partial f_0}{\partial \epsilon}\right) v_z + W(\eta), \text{ etc.} \tag{4.15}$$

Equation (4.14) has the solution $\eta^{(0)} = C^{(0)}(k_z, \epsilon) = \left(-\frac{\partial f_0}{\partial \epsilon}\right)\psi^{(0)}(k_z, \epsilon)$, which is clearly a single-valued function of φ. $\eta^{(1)}$ is single-valued only if

$$\left(-\frac{\partial f_0}{\partial \epsilon}\right) \oint v_z d\varphi = -\oint d\varphi \, W(\eta^{(0)}) \, . \tag{4.16}$$

Note that in general $\oint v_z d\varphi \neq 0$, whereas in the discussion of the transverse magnetoresistance, use was made of the fact that $\oint v_x d\varphi = 0$ for closed orbits. Thus, from Eq. (4.16) it is clear that $\eta^{(0)}$ will generally be non-zero. At magnetic fields sufficiently strong that the higher order terms proportional to $1/H$, $1/H^2$, etc. in η can be neglected, the distribution function is <u>independent of magnetic field and constant around each orbit</u>.

From the definition of $\sigma_{zz}(H)$,

$$\sigma_{zz}(H) = \frac{e^2}{4\pi^3} \int d\vec{k} \, v_z \, \eta \tag{4.17}$$

one can readily show that in the high-field limit

$$\sigma_{zz} \sim \frac{e^2}{4\pi^3} \int d\vec{k} v_z \eta^{(0)} = \frac{e^2}{4\pi^3} \int d\vec{k} \left[-W\left(\eta^{(0)}\right)\psi^{(0)}\right]. \tag{4.18}$$

This is accomplished by changing the integration over wavevector to an integration over orbit variables, making use of Eq. (4.16) and the fact that $\psi^{(0)}$ does not depend upon φ, and then changing back to an integration over wavevector. As one might expect, Eq. (4.18) bears a strong resemblance to Eq. (4.13).

To make the inversion of the conductivity tensor as simple as possible, we assume that the z axis is directed along a twofold or

higher-symmetry axis. In this case $\sigma_{xz}(H) = \sigma_{zx}(H) = \sigma_{yz}(H) = \sigma_{zy}(H) = 0$ and $\rho_{zz}(H) = 1/\sigma_{zz}(H)$. By manipulating Eq. (4·18) suitably, one can write

$$\rho_{zz} = \frac{\frac{1}{4\pi^3}\int d\vec{k}\left[-W\left\{\left(-\frac{\partial f_0}{\partial \epsilon}\right)_{\psi}^{(0)}\right\}_{\psi}^{(0)}\right]}{\left(\frac{1}{4\pi^3}\int d\vec{k} e v_z \left(-\frac{\partial f_0}{\partial \epsilon}\right)_{\psi}^{(0)}\right)^2} \quad . \tag{4·19}$$

This expression has exactly the same form as the variational expression and is in fact just $\rho_v\{\psi^{(0)}\}$. Since $\psi^{(0)}$ will not necessarily be a solution of the zero-field Boltzmann equation, it follows by the variational principle that

$$\rho = \rho_v\{\psi_{H=0}\} \leq \rho_v\{\psi^{(0)}\} \sim \rho_{zz} \quad . \tag{4·20}$$

To summarize, the high-field distribution function is independent of magnetic field and is constant around each orbit. Generally, the zero-field distribution function will vary around each orbit, while the high-field distribution function cannot. According to Eq. (4·20) this can be understood to be the origin of the enhancement of the resistance in a longitudinal magnetic field. In order for no enhancement to occur, $\psi_{H=0}$ and $\psi^{(0)}$ must be the same. In other words, $\psi_{H=0}$ must be constant around each orbit, and Eq. (4·16) must be equivalent to the zero-field Boltzmann equation (Eq. (4·12) with $\omega_c = 0$). This can be the case only if two conditions are satisfied: i) v_z is constant around each orbit, and ii) the scattering rate Q depends only upon the orbit and not upon the position of the electron on it.

D. Application of Semiclassical Transport Theory to Aspects of the Magnetoresistance of Potassium

The magnetoresistance of potassium has puzzled physicists for several decades. In strong magnetic fields the magnetoresistance of potassium increases linearly with field and shows no sign of saturation as predicted by semiclassical theory. While the origin of the

behavior is still not understood,[6] Taub has found recently in this laboratory that the temperature-dependent part of the transverse magnetoresistance, ascribed to electron-phonon scattering, shows a nearly saturating behavior.[7] This suggests that it might be useful to attempt to describe the temperature-dependent part of the transverse magnetoresistance in terms of semiclassical theory.

In Sec. B of this chapter it was shown that $\rho \leq \rho_v\{\tilde{k}_x\} \sim \rho_{xx}$ [Eq. (4·11)]. ρ is the zero-field resistivity, $\rho_v\{\tilde{k}_x\}$ is the variational expression for the zero-field resistivity evaluated using the trial function $\tilde{k}_x$, and ρ_{xx} is the high-field transverse magnetoresistivity. Within the framework of semiclassical transport theory, this relation is valid under the following conditions: i) the metal is cubic and the magnetic field is directed along a twofold or higher-symmetry axis; ii) the Fermi surface consists of closed surfaces, each of which has the above symmetry; and iii) the scattering rate Q is independent of magnetic field. I will assume that these conditions are met. In addition, I assume that the Fermi surface consists of a single closed sheet. Eventually I will assume that the Fermi surface of potassium is spherical, but there is no need to make this assumption at the outset.

Suppose that there are two scattering mechanisms present: impurity and phonon scattering. The collision integral $W(\eta)$ is the sum of the collision integrals for impurity and phonon scattering; i.e. $W(\eta) = W^{imp}(\eta) + W^{ph}(\eta)$.[8] Using the variational expression (Eq. (4·8)), it is possible to write

$$\rho_v\{\tilde{k}_x\} = \rho_v{}^{imp}\{\tilde{k}_x\} + \rho_v{}^{ph}\{\tilde{k}_x\} , \qquad (4·21)$$

where $\rho_v{}^{imp}$ and $\rho_v{}^{ph}$ are the variational expressions associated with W^{imp} and W^{ph}, respectively. Using the additivity of a_{yy} for different scattering mechanisms proved in Sec. IIIB2 and the fact that $\rho_{xx} \sim$

$a_{yy}/(nec)^2$, it follows that

$$\rho_{xx} = \left(\rho_{xx}\right)^{imp} + \left(\rho_{xx}\right)^{ph} , \qquad (4\cdot22)$$

where $\left(\rho_{xx}\right)^{imp}$ and $\left(\rho_{xx}\right)^{ph}$ are the high-field resistivities associated with impurity and phonon scattering, respectively. By Eq. (4·11), one can write

$$\rho_v^{imp}\{\tilde{k}_x\} + \rho_v^{ph}\{\tilde{k}_x\} = \left(\rho_{xx}\right)^{imp} + \left(\rho_{xx}\right)^{ph} . \qquad (4\cdot23)$$

Now I assume that the Fermi surface is spherical and that the impurity scattering is describable by a relaxation time. If this scattering were acting alone, $\tilde{k}_x$ would be (within a constant factor) the actual deviation of the distribution function from equilibrium. However, if impurity scattering is dominant, $\tilde{k}_x$ will still represent the actual distribution function to an excellent approximation. (For a more critical discussion of this point, refer to Appendix D.) Therefore, in the impure limit, $\rho_v\{\tilde{k}_x\}$ should be equal to the actual zero-field resistivity. Furthermore, $\rho_v^{imp}\{\tilde{k}_x\}$ should be temperature independent because the impurity scattering rate is not expected to depend upon temperature. Consequently, $\rho_v^{ph}\{\tilde{k}_x\}$ can be identified with the temperature-dependent part of the resistivity in the impure limit, referred to as ρ_T^{impure}. By subtracting the impurity part ($\rho_v^{imp}\{\tilde{k}_x\} = \left(\rho_{xx}\right)^{imp}$) from Eq. (4·23), one obtains,

$$\rho_T^{impure} = \left(\rho_{xx}\right)_T , \qquad (4\cdot24)$$

where $\left(\rho_{xx}\right)_T = \left(\rho_{xx}\right)^{ph}$ is the temperature-dependent part of the high-field magnetoresistivity. One concludes, therefore, that the temperature dependence of the zero-field resistivity in the impure limit should be identical to the temperature dependence of the magnetoresistivity in the high-field limit.

Note that in principle $\left(\rho_{xx}\right)_T$ can be measured in a sample of any purity because Matthiessen's rule holds in a strong magnetic field (see Sec. IIIB2). Suppose now that one has a sample of arbitrary purity in which one measures the temperature-dependent part of the high-field magnetoresistivity $\left(\rho_{xx}\right)_T$ and the temperature-dependent part of the zero-field resistivity ρ_T. Using Eq. (4·24), one can write that

$$\rho_T^{\text{impure}} - \rho_T = \left(\rho_{xx}\right)_T - \rho_T \quad . \tag{4·25}$$

Thus, deviations from Matthiessen's rule in zero magnetic field, measured by $\rho_T^{\text{impure}} - \rho_T$, should be equal to the enhancement of the resistivity, $\left(\rho_{xx}\right)_T - \rho_T$, produced by a strong magnetic field.[9]

Similar predictions can be made for the temperature-dependent part of the longitudinal magnetoresistance. Without going through the arguments, which are analogous to those just given, one finds that

$$\rho_T^{\text{impure}} = \left(\rho_{zz}\right)_T^{\text{impure}} \quad . \tag{4·26}$$

Deviations from Matthiessen's rule can be expected to occur for the high-field longitudinal magnetoresistance because for this situation the distribution function depends upon the nature of the scattering mechanism.

REFERENCES

1. L. D. Landau and E. M. Lifshitz, Statistical Physics, (Addison-Wesley Publishing Company, Hungary, 1969), Sec. 54.
2. This is shown in a different manner in J. M. Ziman, Electrons and Phonons, (Oxford University Press, Oxford, 1960), Sec. 12.6.
3. Ibid. Sec. 7.7.
4. It is not obvious that Eq. (3·26) is also valid when the magnetic field is along a threefold symmetry axis. A simple proof based on the arguments given in Appendix C can be constructed.
5. There has been some confusion on this point. In an article by W. A. Harrison in The Fermi Surface, edited by W. A. Harrison and M. B. Webb (John Wiley and Sons, Inc., New York, 1960), p. 37, Harrison shows the electron and hole distribution functions "shifted" in opposite directions in $\vec{k}$-space in a magnetic field. A careful look at the diagram shows that it has been drawn incorrectly.
6. For a detailed discussion of previous work and for an account of extensive measurements in potassium, see H. Taub, R. L. Schmidt, B. W. Maxfield, and R. Bowers, Phys. Rev. B 4, 1134 (1971).
7. H. Taub and D. K. Wagner (to be published).
8. This is not an assumption of Matthiessen's rule. It is a statement of the fact that the total scattering probability should be the sum of the probabilities associated with the two separate scattering mechanisms.
9. This result has also been derived by M. Kohler, Ann. Physik 38, 283 (1940) for a free electron gas undergoing only normal electron-phonon collisions. The analysis presented in this thesis is valid for both normal and umklapp processes.

CHAPTER V

The RF Size Effect in Potassium

A. Introduction

The rf size effect was discovered experimentally by Gantmakher in 1962.[1] Since that time the effect has been observed and studied in a number of metals.[2] As a transport process, the rf size effect has been the subject of considerable intrinsic interest. In addition it has proved to be a powerful tool for measuring Fermi surfaces and a useful technique for investigating electron mean-free paths.

This chapter is concerned with assessing the feasibility of using the rf size effect to detect anisotropies of the electron mean-free path in potassium. In Sec. B, the current understanding of the rf size effect for a spherical Fermi surface is summarized, and an experiment for detecting ansitropies in the electron mean-free path is proposed. In Sec. C the experimental aspects of this proposal are considered and some preliminary results are presented. A final assessment of the proposal is given in Sec. D.

It is useful to review briefly the rf size effect work that has been done to date in potassium. Koch and Wagner[3] were the first to study the effect in potassium, and their study was concerned mainly with understanding the magnetic field values at which the surface impedance anomalies occur. Subsequently, Peercy et al.[4] extended their study with improved experimental technique and presented a geometrical model that correctly predicts the magnetic field positions of the surface impedance anomalies. Once the spectroscopic aspects of the rf size effect were understood, investigations of the electron mean-free path by means of the rf size effect became feasible. A study of the temperature dependence of the electron mean-free path in potassium was made by Tsoi and Gantmakher.[5] A somewhat broader study was made by Blaney and Parsons[6] who made measurements on both poly- and single-

crystal specimens. In their experiment they measured a temperature-dependent mean-free path that is in good agreement (within 15%) with that measured by Tsoi and Gantmakher, but observed no anisotropy in the electron mean-free path; that is, they observed that the temperature-dependent mean-free path was essentially the same from sample to sample. Unfortunately, no information about sample orientation, or even the number of samples measured is given, so that it is difficult to critically evaluate their conclusion that there was no anistropy. It seems that this conclusion could be tested more sensitively by performing measurements on a single sample (a single crystal), whose orientation could be varied. This forms the basis for the experiment proposed in the next section.

Calculations of the shapes of the rf surface impedance anomalies have been performed by Kaner and Falko[7] and more recently by Juras.[8] While these calculations are interesting in their own right, much information about the rf size effect can be gotten from simpler considerations, as discussed in the next section.

B. The RF Size Effect

1. The Electron Trajectories

In order to understand how the rf size effect can be used to measure electron mean-free paths, it is necessary first to understand how the rf surface impedance anomalies arise, and in particular which electron trajectories are responsible for a given anomaly. A very complete explanation of the rf size effect in potassium has been given by Peercy et al.[4] We give a discussion of the relevant aspects of their treatment below.

The rf size effect can be observed most simply in a thin plate of pure metal of thickness d, oriented with a static magnetic field $\vec{H}$ parallel to the surface. An rf electric field polarized perpendicular to $\vec{H}$ and parallel to the surface acts to accelerate electrons in the

skin depth. If the electron mean-free path ℓ is on the order of the plate thickness d, many of these electrons will follow trajectories into the bulk of the metal, and some may reach the other side of the plate. Under certain circumstances, these electrons can make a significant contribution to the rf currents in the skin depth, and can cause a change in the rf surface impedance of the plate. It is the changes in the rf surface impedance, generally as a function of magnetic field, that is the principal observable consequence of the rf size effect.

There are three conditions that must be met in order for a change in the surface impedance to occur. Firstly, the electrons responsible for the change in surface impedance must follow trajectories that just span the thickness of the plate from skin depth to skin depth. Secondly, the electrons must be travelling parallel to the surface in each skin depth in order to make an effective contribution to the rf skin currents and hence to the surface impedance. Thirdly, there must be an abrupt change in the number of such electrons to cause a change in the surface impedance. To illustrate this concretely, we consider possible electron trajectories for a spherical Fermi surface as the magnetic field is increased from zero.

At a small finite value of the magnetic field, a small number of electrons with non-extremal orbits on the Fermi surface will have trajectories that just span the thickness of the plate and pass through both skin layers travelling parallel to the surface. Although these electrons will make a contribution to the rf current in the skin depth, there are always a small number of such electrons at neighboring field values, so that no measurable change in the surface impedance with magnetic field will result. However, at the field H_o such that the trajectories of the electrons on the extremal belt of the Fermi surface just span the thickness of the plate, a large group of electrons having nearly the same orbit diameter contribute to the currents in the skin

depth and a change in the surface impedance will result. It is important to note that this group of electrons has trajectories that are focussed in the opposite skin depth; that is, a first order change in the $\vec{K}$-space orbit produces only a second order change in the depth of the trajectory. As the magnetic field is increased further, the surface impedance anomaly will persist until the trajectories of the electrons on the extremal belt of the Fermi surface no longer intersect both skin depths. Consequently, the fractional width $\Delta H/H$ of the anomaly will be on the order of $2\delta/d$, where δ is the skin depth.

At fields larger than H_o, other surface impedance anomalies can occur, but via a different mechanism. For example, at the field $2H_o$, the electrons on the extremal belt of the Fermi surface which pass through the skin depth on one side of the plate will carry current into the bulk of the metal and will form a current sheet at a depth of roughly $d/2$. The fields associated with this current sheet can in turn accelerate electrons which produce currents in the skin depth on the opposite side of the plate. Thus, chains of trajectories linking the sample surfaces become possible and cause changes in the surface impedance at multiples of the fundamental field H_o.

A more complicated, but interesting situation occurs when the static magnetic field $\vec{H}$ is tilted out of the sample plane by an angle φ. It is customary to arrange the polarization of the rf electric field either perpendicular to the magnetic field $\vec{H}$ and parallel to the sample surface or along the projection of the magnetic field in the plane of the sample surface. One should note, however, that the polarization of the rf electric field is of no importance in determining the positions of the rf surface impedance anomalies; rather, it serves only to emphasize certain anomalies. For example, the perpendicular polarization emphasizes anomalies due to electrons near the extremal belt of the Fermi surface, since these electrons have velocities directed along the rf field as they pass through the skin depth. Instead

of discussing each polarization separately, it is much more convenient to assume that all polarizations are present. This is the approach used in the following discussion.

It is useful to introduce some concepts used by Peercy, et al. The term "effective" electrons is used to mean those electrons travelling parallel to the surface in the skin depth. In this connection the term "effective point" is used to mean that point on the electron trajectory at which the velocity is parallel to the surface. For a spherical Fermi surface it is possible to unambiguously label an orbit on the Fermi surface by the angle θ, measured with respect to the direction of the magnetic field $\vec{H}$. The point on the Fermi surface corresponding to the point $\theta = 0$ is referred to as the "limiting point".

Peercy et al. have derived analytic expressions in terms of θ and φ for the onset fields of the surface impedance anomalies. While the calculations are straightforward exercises in analytic geometry, their interpretation is not so transparent. A great deal can be learned, however, from a simple picture of the possible orbits in $\vec{k}$-space and the corresponding trajectories in real space. In Figure 5.1 the effective points on the Fermi surface are shown; they lie on the great circle formed by the intersection of the Fermi sphere with a plane parallel to the sample surface. The $\vec{k}$-space orbits are confined to the intersection of the Fermi sphere with planes perpendicular to the magnetic field $\vec{H}$. Since the electron trajectories must have an effective point in each skin depth to cause a surface impedance anomaly, the $\vec{k}$-space orbits must begin and end on one of the effective points indicated on the Fermi sphere. In Figure 5.1 a possible orbit is indicated, beginning at point 1 and ending at point 2. If the magnetic field strength H and angles θ and φ are chosen correctly, the real space trajectory will have an effective point in each skin depth as indicated in Figure 5.1. Note that there are no effective points for electrons with $\theta < \varphi$. These electrons will always be ineffective

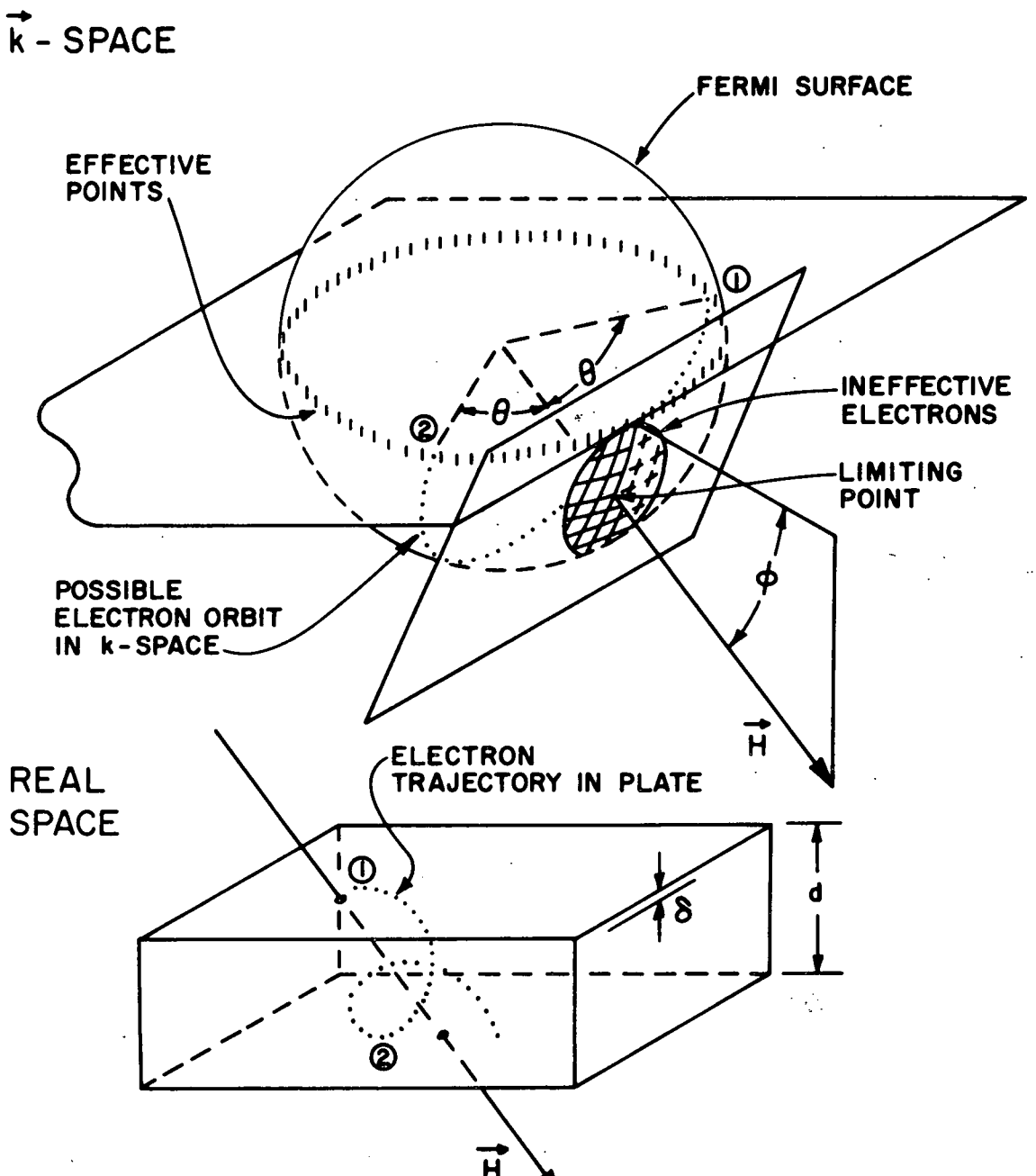

Figure 5.1 Perspective drawing of a possible electron orbit in $\vec{k}$-space and the corresponding electron trajectory in real space.

and therefore play a minimal role in the rf size effect.

In the discussion of the parallel-field effect, it was convenient to consider the changes in the rf surface impedance as the magnetic field was increased from zero. It is also useful to do the same for the tilted-field effect. At a small value of the magnetic field, a small number of electrons with $\theta < \varphi$ will have trajectories which just span the plate. Since these electrons have no effective points on their orbits, they will make a minimal contribution to the rf surface impedance. However, as the magnetic field is increased further, electrons on the limiting point orbit ($\theta = \varphi$) will just span the thickness of the plate. Since these electrons have an effective point on the orbit, they can contribute significantly to the rf surface impedance, and a change in the surface impedance will result. It is the change from ineffective to effective behavior that is responsible for this surface impedance anomaly.

The next surface impedance anomaly occurs at a field slightly greater than H_o and is due to the focussing of the trajectories of electrons near the extremal belt of the Fermi surface into the skin depth on the opposite side of the plate. At higher fields, current sheets within the bulk of the metal can be formed, and chains of trajectories become possible. This aspect of the rf size effect is discussed in detail in the article by Peercy *et al*.

From the standpoint of measuring electron mean-free paths, it is the limiting point orbit that is of the greatest interest. It is this orbit that samples the smallest portion of the Fermi surface, and which therefore should yield information about scattering on a localized area of the Fermi surface. By using some analytic geometry it is not difficult to show that the onset field of the limiting point anomaly is given by

$$H = H_o\left(\frac{\pi}{2} \sin 2\varphi\right) . \qquad (5\cdot1)$$

Thus, H is less than H_0 for tilt angles φ less than about 20°. Also one can show that the length of the trajectory L between effective points is

$$L = 2d/\sin 2\varphi \quad . \tag{5.2}$$

If the scattering events are random and have the same effect at each point on the orbit, it is clear that the amplitude A of the surface impedance anomaly should vary as

$$A \propto \exp(-L/\ell) = \exp(-2d/\ell \sin 2\varphi) \quad . \tag{5.3}$$

In principle, the mean-free path ℓ can be deduced by measuring the variation of the amplitude A as a function of tilt angle φ. This method has been used by Tsoi and Gantmakher[5] and Blaney and Parsons[6] to measure the electron mean-free path.

2. The Electron Mean-Free Path

At this stage in the discussion it is important to clarify just what is meant by the electron mean-free path. This matter is by no means as simple as it may seem; it is sobering to consider the fact that in almost every real situation it is impossible to rigorously define a relaxation time or a mean-free path. Even if one tries to approximately define a relaxation time or a mean-free path, one generally will find that its value will depend upon the transport property being investigated.

Our understanding of transport processes in metals rests on the Boltzmann equation for the distribution function f. In this equation the time rate of f due to scattering has the form

$$-\left(\frac{\partial f}{\partial t}\right)_{\text{scatt.}} = \frac{1}{k_B T} \frac{1}{4\pi^3} \int d\vec{K}(\psi - \psi') P(\vec{K},\vec{K}') \quad , \tag{5.4}$$

which is the same as Eq. (3.5). Again $(-\partial f_0/\partial \varepsilon)\psi$ is proportional to the deviation of the distribution function from equilibrium, and $P(\vec{K},\vec{K}')$

is the equilibrium transition rate between the states of wavevector $\vec{K}$ and $\vec{K}'$ allowing for occupation of these states and is equal to $f_0(\epsilon)(1-f_0(\epsilon'))Q(\vec{K},\vec{K}')$. $Q(\vec{K},\vec{K}')$ is the corresponding transition rate disregarding the occupation of the initial and final states.

A relaxation time τ exists only if one can show that $-(\partial f/\partial t)_{scatt.} = (-\partial f_0/\partial \epsilon)\psi/\tau$ for all transport processes; that is, for all possible ψ. This will generally occur for only special transition rates. For example, if the scattering is elastic and isotropic (i.e. $Q(\vec{K},\vec{K}') = \delta(\epsilon-\epsilon')\cdot$const.) a relaxation time will exist. However, in this discussion it is profitable to take a more limited view. Consequently, we shall concern ourselves mainly with experiments, like the rf size effect, in which ψ is appreciable only on a small area of the Fermi surface. If the angular region $\Delta\theta$ over which ψ is appreciable is smaller than the characteristic angle of scatter, then the second term in the collision integral (Eq. (5·4)) can be neglected with respect to the first. In this case one obtains a relaxation time $\tau(\vec{K})$ given by

$$\frac{1}{\tau(\vec{k})} = \frac{1}{4\pi^3}\int \frac{f_0(\epsilon')}{f_0(\epsilon)} Q(\vec{K}',\vec{K})d\vec{K}', \qquad (5\cdot5)$$

and a mean-free path $\ell(\vec{K}) = \tau(\vec{K})v(\vec{K})$. This approximation amounts to neglecting the scattering into the regions in which ψ is appreciable with respect to the scattering out of these regions. Or stated differently, in this approximation every collision is viewed as catastrophic in the sense that it will remove an electron from the group responsible for the surface impedance anomaly.

Is this approximation justified for electron-phonon scattering in potassium? Unfortunately, it is justified only marginally at best. To see this, one must estimate the angular range over which ψ is appreciable and compare this with the characteristic electron-phonon scattering angle. In the case of focussed trajectories, ψ should be appreciable over an angular range $\Delta\theta$ on the order of $\sqrt{\delta/d}$, since a

change in the $\vec{K}$-space orbit by this amount will produce a fractional change in the depth of the trajectory of roughly δ/d. In the case of the unfocussed trajectory corresponding to the limiting point orbit for $\varphi < 20^{\circ}$, it seems that the angular range $\Delta\theta$ should be on the order of δ/d. The characteristic angle of scattering for normal electron-phonon collisions is on the order of (T/θ_D), which for potassium at 1 K is about 10^{-2}. (Umklapp electron-phonon collisions are not an important consideration here because they will be catastrophic). Since δ/d is typically also about 10^{-2}, the argument that a typical electron-phonon collision will render the electron ineffective is rather tenuous for the limiting point orbit and implausible for the focussed orbits.

Both Tsoi and Gantmakher[5] and Blaney and Parsons[6] have pointed out this difficulty. The experiments, however, give a $1/T^3$ dependence of the electron-phonon mean-free path which suggests that each electron-phonon collision is catastrophic. Actually, this is probably not the case; it is more likely that the $1/T^3$ dependence arises from the fact that a collision which is not catastrophic makes only a small contribution to the collision integral due to the near cancellation of $(\psi-\psi')$ in the integrand. Thus only a fraction of the collisions will actually determine the value of the collision integral (Eq. (5·4)). As a result, the mean-free path deduced from the rf size effect experiment can be expected to be considerably larger than that which would be measured if <u>all</u> electron-phonon collisions were catastrophic. In fact, both Tsoi and Gantmakher and Blaney and Parsons do find that the electron-phonon mean-free path deduced from the rf size effect is about an order of magnitude larger than that estimated from the dc electrical resistivity. In contrast, they find that the electron-impurity mean-free path deduced from the rf size effect is in good agreement with that estimated from the dc electrical resistivity.

In summary, it is difficult to claim that a unique electron-phonon relaxation time given by Eq. (5·4) will be measured in an rf

size-effect experiment. Consequently, the value of the electron-phonon mean-free path deduced from the experiment may depend upon the particular surface impedance anomaly being studied, and this should be kept in mind when interpreting the results.

3. Proposed Experiment

Despite the fact that a mean-free path for electron-phonon scattering may not be well defined in an rf size-effect experiment, it is still possible to use the effect to detect anisotropies in the scattering. In this case one measures in some sense an average of the collision integral over the orbit responsible for the surface impedance anomaly. The value of this average can be expected to vary with crystallographic orientation if the electron-phonon scattering rate $Q(\vec{k},\vec{k}')$ is anisotropic. Because of the importance of umklapp electron-phonon scattering near the <110> zone faces in potassium, such anisotropy can be expected to be present in potassium at low temperatures.

The most straightforward method for detecting an anisotropy in the electron-phonon scattering is to measure the amplitude A of the limiting point surface impedance anomaly as a function of crystalline orientation for different temperatures. A number of crystalline orientations can be sampled by rotating the magnetic field about the normal to the sample surface. In the conventional experimental arrangement, a rectangular coil is used to produce the rf electric field, and this coil would have to be rotated with the magnetic field to maintain constant coupling with the electrons in the skin depth. This can be a severe disadvantage, however, because it would be difficult to rotate such a coil without disturbing the sample. Even if this could be arranged, it would be difficult to maintain the same separation between the coil and sample surface, and this could cause considerable ambiguity in the results. All of these difficulties can be overcome by using spiral coils, used extensively in acoustic work in this laboratory,[9]

to generate an rf electric field with circular symmetry in the plane of the sample surface. With spiral coils, both the sample and spiral coils can be fixed, allowing measurement of the amplitude of the limiting point anomaly as a function of crystalline orientation by rotation of the static magnetic field alone.

C. Experimental Technique and Some Preliminary Results

The preliminary measurements were made with the conventional rectangular coil and with a pair of spiral coils, wired in series opposition, with the sample placed between them. With each coil arrangement it was possible to detect the first three surface impedance anomalies at H_o, $2H_o$, and $3H_o$ for the static magnetic field parallel to the surface. No attempt was made to detect the surface impedance anomalies in a tilted field because this could not be done easily with the apparatus used. In any event, these preliminary measurements showed clearly that the observation of the rf size effect in thin potassium plates is not difficult, so that the extension of these measurements to tilted fields and single-crystal potassium plates should be straightforward.

It is useful to describe the experimental technique briefly. A 0.2- to 0.3-mm thick pressed plate of potassium was placed either inside a rectangular coil, or was sandwiched between two spiral coils, and the coil arrangement was placed in one arm of a twin-T bridge.[10] The bridge was driven at 32 MHz and the output amplified by 40 db, mixed with the bridge drive signal, and filtered. Thus, any deviations of the bridge output from balance caused by changes in the rf surface impedance would appear as a dc voltage after filtering. To further enhance the signal/noise, the static magnetic field was modulated at 23 Hz and the filtered output of the mixer was phase-sensitively detected at this frequency. The full-scale sensitivity was about 0.2 μV referred to the output of the twin-T bridge for an integration time of 1 second.

This system seems quite adequate for future measurements. At the present time, a superconducting magnet system is being built that will allow rotation of the magnetic field while maintaining a constant tilt angle φ. This magnet system will consist of a solenoid and a pair of Helmholtz coils. The solenoid will produce a vertical field, and the Helmholtz pair will produce a horizontal field that can be rotated in the horizontal plane by rotating the Helmholtz pair. Thus, if the sample surface is horizontal, the solenoid can be used to generate a constant tilt angle. Then by rotating the Helmholtz pair, the limiting point can be moved in a full circle around the Fermi surface.

D. Summary

In summary, it can be concluded that a measurement of the electron-phonon scattering anisotropy by means of the rf size effect is feasible in potassium. By using spiral coils which produce all polarizations of the rf electric field in the plane of the sample surface, different crystallographic directions can be sampled by simple rotation of the static magnetic field alone. By this method the problem of comparing measurements in different samples is entirely avoided. It should not be difficult to achieve resolution of anisotropies in the scattering of several percent, and, keeping in mind the cautionary remarks in Sec. B2, this experiment should yield useful information about electron-phonon scattering in potassium.

REFERENCES

1. V. F. Gantmakher, Zh. Eksperim. i Teor. Fiz. 42, 1416 (1962); 43, 345 (1962); 44, 811 (1963) [Sov. Phys. JETP 15, 982 (1962); 16, 247 (1962); 17, 549 (1963)].
2. For a comprehensive review of the rf size effect, see the review article by V. F. Gantmakher in Progress in Low-Temperature Physics, edited by C. J. Gorter (North-Holland Publishing Co., Amsterdam, 1967), p. 181.
3. J. F. Koch and T. K. Wagner, Phys. Rev. 151, 467 (1966).
4. P. S. Peercy, W. M. Walsh, Jr., L. W. Rupp, Jr., and P. H. Schmidt, Phys. Rev. 171, 713 (1968).
5. V. S. Tsoi and V. F. Gantmakher, Zh. Eksperim. i Teor. Fiz. 56, 1232 (1969) [Sov. Phys. JETP 29, 663 (1969)].
6. T. G. Blaney and D. Parsons, J. Phys. C. Proc. Phys. Soc. (Solid State Physics) 3, 126 (1970).
7. E. A. Kaner and V. L. Falko, Zh. Eksperim. i Teor. Fiz. 51, 586 (1966) [Sov. Phys. JETP 24, 392 (1967)].
8. G. E. Juras, Phys. Rev. 187, 784 (1969).
9. M. R. Gaerttner, Ph. D. Thesis, Cornell University, 1971.
10. H. L. Anderson, Phys. Rev. 76, 1460 (1949).

APPENDIX A

Computation of the Thermal Resistivity from the Experimental Data

The quantities measured in the experiment are $R_1(T)$, $\Delta R(T, \Delta T)$, $\Delta R(T, 0)$, and $\dot{Q}$. By expanding $R_2(T + \Delta T)$ in a Taylor series in ΔT about T, it follows that,

$$\Delta R(T, \Delta T) - \Delta R(T, 0) = -R_2'(\Delta T) - \tfrac{1}{2}R_2''(\Delta T)^2 + \ldots \qquad (A\cdot1)$$

where $R_2' = dR_2/dT$ and $R_2'' = d^2R_2/dT^2$. The quadratic term in Eq. (A·1) is typically less than 1% of the linear term for temperature differences less than 30 mK. Thus to first order, the quadratic term can be ignored. In this approximation ΔT is given by

$$\Delta T = -\frac{\Delta R(T, \Delta T) - \Delta R(T, 0)}{R_2'} \quad . \qquad (A\cdot2)$$

The derivative R_2' is calculated from an analytical fit of the resistance data. I have found it convenient to fit the data to the formula of Clement and Quinell:[34]

$$\frac{1}{T} = \frac{a_{-1}}{\log R_2} + a_0 + a_1 \log R_2 \quad . \qquad (A\cdot3)$$

The data is divided into two temperature ranges: 1.5 to 4.0 K and 3.5 to 6.5 K. The data in each range is fit by using the two points at each end of the range and one point in the center of the range to determine the three coefficients a_{-1}, a_0, and a_1. The fits obtained in this manner compare favorably with those obtained by a least-squares method. The systematic deviations of the data from the fit are always less than 5 mK. The first derivative R_2' is obtained by differentiating Eq. (A·3) with respect to temperature. One obtains,

$$R_2' = R_2 \frac{1}{T^2} \cdot \frac{\log R_2}{\dfrac{a_{-1}}{\log R_2} - a_1 \log R_2} \qquad (A\cdot4)$$

In practice Eq. (A·3) is used to calculate T from the measured value of $R_2(T) = R_1(T) - \Delta R(T, 0)$. Then Eqs. (A·2) and (A·4) are used to calculate ΔT.

There are two sources of systematic error in this method: the first arises from the neglect of the small quadratic term in Eq. (A·1), and the second from the fact that the actual temperature and the temperature that one calculates by Eq. (A·3) differ by a small amount $\epsilon(T)$ due to the difficulty of fitting the data within the experimental error.

In the first case the effect of the quadratic term is to multiply ΔT by the factor $(1 - \frac{1}{2}\frac{R_2''}{R_2'}(\Delta T))$. The second derivative R_2'' can be calculated from Eq. (A·4). One obtains

$$\frac{R_2''}{R_2'} = -\frac{2}{T} + \left(\frac{R_2'}{R_2}\right)\left[1 + \frac{2a_{-1}T^2}{(\log R_2)^3}\left(\frac{R_2'}{R_2}\right)\right] . \qquad (A·5)$$

In the second case the effect of $\epsilon(T)$ on WT can be calculated by replacing T in Eq. (A·3) by $T - \epsilon(T)$. One finds that to first order in ϵ the actual value of WT is obtained by multiplying the calculated value of WT by $(1 - \frac{\epsilon}{T} + \frac{d\epsilon}{dT})$. Typically I find that $|\frac{d\epsilon}{dT}| < .02$ and $|\frac{\epsilon}{T}| < .002$. The quantity ϵ and its derivative can be determined with a precision of about 40%. Consequently, after making these corrections, it is possible to reduce the total systematic error in the thermal resistivity to a value of less than one percent.

APPENDIX B

Proof that $C_E^{(0)}(k_z,\varepsilon) = (-\partial f_0/\partial\varepsilon)\cdot\text{const.}$

In this appendix I wish to show that $C_E^{(0)}(k_z,\varepsilon) = (-\frac{\partial f_0}{\partial\varepsilon})\cdot\text{const.}$ Since the distinction between electrical and thermal conduction is unimportant, I drop the E and T subscripts on η and ψ. First in i), I prove the result for only intraband scattering. Next in ii), I indicate how the argument is extended to two bands with combined intra- and interband scattering.

i) Multiplying Eq. (3·12) by $(-eH/\hbar^2 c\omega_c)dk_z d\varepsilon\psi^{(0)}$, integrating over k_z and ε, noting that $\psi^{(0)}$ is <u>not</u> a function of φ gives

$$-\frac{eH}{\hbar^2 c}\int\frac{dk_z}{\omega_c}\int d\varepsilon\oint d\varphi W(C^{(0)})\psi^{(0)} = 0 \ . \qquad (B\cdot1)$$

However, $d\vec{k} = (-eH/\hbar^2 c\omega_c)dk_z d\varepsilon d\varphi$, so that the integration may be changed back to an integration over wave vector. Using Eq. (3·5) for the collision integral, one obtains

$$\oint d\vec{k}\int d\vec{k}'\left[\psi^{(0)} - \psi^{(0)'}\right]^2 P(\vec{k},\vec{k}') = 0 \ . \qquad (B\cdot2)$$

Since the integrand is always positive, this condition can be met only if $\psi^{(0)} = \text{const.}$, or $C^{(0)}(k_z,\varepsilon) = (-\frac{\partial f_0}{d\varepsilon})\ \text{const.}$

A similar proof can be constructed for electron-electron scattering by using Eq. (3·7) for the collision integral.

ii) Following the discussion in Sec. IIIB2, I denote the two bands by α and β. The quantities $C_\alpha^{(0)}$ and $C_\beta^{(0)}$ are determined by the two conditions:

$$\oint d\varphi_\alpha W_\alpha(C_\alpha^{(0)};C_\beta^{(0)}) = 0 \quad\text{and}\quad \oint d\varphi_\beta W_\beta(C_\beta^{(0)};C_\alpha^{(0)}) = 0. \qquad (B\cdot3)$$

Multiplying the first equation by $(-eH/\hbar^2 c\omega_{c\alpha})dk_{z\alpha}d\epsilon_\alpha\psi_\alpha^{(0)}$, the second by $(-eH/\hbar^2 c\omega_{c\beta})dk_{z\beta}d\epsilon_\beta\psi_\beta^{(0)}$, adding the resulting equations, and changing the integrations back to integrations over wave vector, one obtains for impurity or electron-phonon scattering,

$$\tfrac{1}{2}\int_\alpha d\vec{K}\int_\alpha d\vec{K}'(\psi_\alpha^{(0)}-\psi_\alpha^{(0)'})^2 P_{\alpha\alpha}(\vec{K},\vec{K}') + \tfrac{1}{2}\int_\beta d\vec{K}\int_\beta d\vec{K}'(\psi_\beta^{(0)}-\psi_\beta^{(0)'})^2 P_{\beta\beta}(\vec{K},\vec{K}')$$

$$+ \int_\alpha d\vec{K}\int_\beta d\vec{K}'(\psi_\alpha^{(0)}-\psi_\beta^{(0)'})^2 P_{\alpha\beta}(\vec{K},\vec{K}') = 0 \qquad (B\cdot 4)$$

where use has been made of the symmetry properties of the P's. Since each term is positive definite, this condition can be satisfied only if each term vanishes separately. Therefore, $\psi_\alpha^{(0)} = \psi_\beta^{(0)} = \text{const.}$ The extension to electron-electron scattering is straightforward, though tedious.

APPENDIX C

Proof that $\eta(\varphi + \pi) = -\eta(\varphi)$

I wish to show that if the magnetic field $\vec{H}$ is directed along a twofold symmetry axis and the orbits have this same symmetry, that the solution η to the Boltzmann equation has the property $\eta(\varphi + \pi) = -\eta(\varphi)$. For simplicity consider electrical transport and intraband scattering given by the collision integral of Eq. (3·5). Let $\vec{k}_r$ and $\vec{k}_r'$ be the vectors corresponding to a rotation of π about $\vec{H}$ of $\vec{k}$ and $\vec{k}'$. At $\vec{k}_r$, corresponding to the point $(\varphi + \pi)$ on the orbit, the collision integral $W_r(\eta(\varphi + \pi))$ is

$$- \frac{1}{k_B T} \frac{1}{4\pi^3} \int d\vec{k}_r' \left[\psi(\varphi + \pi) - \psi'(\varphi + \pi) \right] P(\vec{k}_r, \vec{k}_r'). \qquad (C \cdot 1)$$

However, $P(\vec{k}_r, \vec{k}_r') = P(\vec{k}, \vec{k}')$ by virtue of the twofold rotational symmetry and $d\vec{k}_r' = d\vec{k}'$. Consequently, $W_r(\eta(\varphi + \pi)) = W(\eta(\varphi + \pi))$. This last result also holds for electron-electron scattering, which can be verified by repeating the same argument using Equation (3·7) for the collision integral. Utilizing the fact that $v_x(\varphi + \pi) = -v_x(\varphi)$, the Boltzmann equation for $\eta(\varphi + \pi)$ can be written

$$\omega_c \frac{\partial \eta(\varphi + \pi)}{\partial \varphi} = -\left(- \frac{\partial f_0}{\partial \varepsilon} \right) v_x(\varphi) + W(\eta(\varphi + \pi)). \qquad (C \cdot 2)$$

Adding this equation to Eq. (3·4) for $\eta(\varphi)$, and letting $\eta_+ = \frac{1}{2}\left[\eta(\varphi) + \eta(\varphi + \pi) \right]$, one obtains

$$\omega_c \frac{\partial \eta_+}{\partial \varphi} = W(\eta_+) \qquad (C \cdot 3)$$

subject to the condition that η_+ be a single-valued function of φ. Note that η_+ satisfies the same equation, subject to the same boundary condition, that is satisfied by $f - f_0$ in the absence of an electric

field. Since $f - f_0$ is zero in this situation, and this solution is unique, η_+ must be zero. Therefore, $\eta(\varphi + \pi) = -\eta(\varphi)$. This property depends only upon the symmetry properties of the collision integral and is valid for interband as well as intraband scattering. For thermal transport a similar argument can be constructed.

APPENDIX D

A Discussion of the Solution to the Zero-Field Boltzmann Equation when the Dominant Scattering Mechanism is Describable by a Relaxation Time

I assume two scattering mechanisms: one which can be described by a relaxation time τ and the other which cannot. The collision integral for the former is $-\eta/\tau$ and for the latter, $W(\eta)$. Thus, the zero-field Boltzmann equation is

$$\left(-\frac{\partial f_0}{\partial \varepsilon}\right)v_x = \eta/\tau - W(\eta). \tag{D·1}$$

I assume that the scattering mechanism describable by the relaxation time is dominant, so that as a first approximation $W(\eta)$ can be ignored with respect to η/τ. In this approximation

$$\eta_0 = \left(-\frac{\partial f_0}{\partial \varepsilon}\right)v_x\tau. \tag{D·2}$$

Iterating Eq. (D·1) yields

$$\eta_1 = \eta_0 + \tau W(\eta_0), \tag{D·3}$$

$$\eta_2 = \eta_1 + \tau W[\tau W(\eta_0)], \text{ etc.} \tag{D·4}$$

Assuming the crystal is cubic, the conductivity σ is just

$$\sigma = \frac{e^2}{4\pi^3}\int d\vec{k}\; v_x\eta$$

$$= \sigma_0 + \frac{e^2}{4\pi^3}\int d\vec{k}\; \tau v_x W(\eta_0) + \ldots, \tag{D·5}$$

where

$$\sigma_0 = \frac{e^2}{4\pi^3}\int d\vec{k}\; v_x\eta_0 = \frac{e^2}{4\pi^3}\int d\vec{k}\; v_x\left(-\frac{\partial f_0}{\partial \varepsilon}\right)v_x\tau\,. \tag{D·6}$$

Now $\rho = 1/\sigma$. Assuming that the term containing $W(\eta_o)$ in Eq. (D·5) is small compared to σ_o, one obtains,

$$\rho = \rho_o + \frac{\frac{1}{4\pi^3}\int d\vec{k}\left[-W\left\{\left(-\frac{\partial f_0}{\partial \epsilon}\right)\psi_o\right\}\psi_o\right]}{\left(\frac{1}{4\pi^3}\int d\vec{k}\, ev_x\left(-\frac{\partial f_0}{\partial \epsilon}\right)\psi_o\right)^2}, \qquad (D\cdot 7)$$

with $\psi_o = v_x\tau$ and $\rho_o = 1/\sigma_o$. The second term in Eq. (D·7) is the variational expression $\rho_v\{\psi_o\}$. Therefore, I have shown that <u>when the scattering describable by a relaxation time dominates, the contribution of the scattering mechanism not describable by a relaxation time can be calculated using the variational expression with the relaxation-time trial function</u>.

The meaning of the use of the term "dominant" can be made more precise by calculating the terms of higher order in Eq. (D·7). One requires that these terms be small relative to the second term in Eq. (D·7). Specifically,

$$\left| \frac{\rho_v\{\psi_o\}}{\rho_o} - \frac{\frac{1}{4\pi^3}\int d\vec{k}\left[-W\left\{-\tau W\left[\left(-\frac{\partial f_0}{\partial \epsilon}\right)\psi_o\right]\right\}\psi_o\right]}{\frac{1}{4\pi^3}\int d\vec{k}\left[-W\left\{\left(-\frac{\partial f_0}{\partial \epsilon}\right)\psi_o\right\}\psi_o\right]} \right| \ll 1 . \qquad (D\cdot 8)$$

Unfortunately, this expression is so complicated that it seems to be of little practical value. However, it is clear that the onset of the regime in which the scattering mechanism describable by a relaxation time is dominant depends both upon the nature of the collision integral $W(\eta)$ and its magnitude. In many respects the difficulty in defining the onset of this regime is similar to the difficulty in defining the onset of the high-field regime.